Radar Attenuation for Subsurface Sounding on Enceladus: Effects of a Porous Ice Layer

William Paul Byrne[1], Ana-Catalina Plesa[1], Tina Rückriemen[1], Hauke Hussmann[2], and Andreas Benedikter[1]

[1]German Aerospace Center
[2]DLR, Institute for Planetary Research

April 23, 2024

Abstract

The presence of a global ocean, the water-rock interface at the base of the ocean, and the inferred ocean composition derived from sampling the active plume at the south pole of Enceladus, make Saturn's moon a promising location for habitable conditions in the Solar System. Due to its thin (<35 km) and cold ice shell, Enceladus is expected to exhibit favourable conditions for direct detection of the ice-ocean interface using low-frequency radar sounder instruments. Here we investigate the two-way radar attenuation in the Enceladus ice shell, focusing on the effect of a porous icy layer generated by Enceladus' jet activity. Our results show that as little as 2% of the ice shell can be penetrated in regions covered by thick and strongly insulating porous layers. However, the high subsurface temperatures in these regions could promote the formation of brines at shallow depth that can be detected by future radar measurements.

Radar Attenuation for Subsurface Sounding on Enceladus: Effects of a Porous Ice Layer

William Byrne[1,2], Ana-Catalina Plesa[1], Tina Rückriemen-Bez[1], Hauke Hussmann[1], Andreas Benedikter[3]

[1]Institute of Planetary Research, German Aerospace Center (DLR), Rutherford Str. 2, 12489 Berlin, Germany
[2]University of Maryland, College Park, MD 20742, USA
[3]Microwaves and Radar Institute, German Aerospace Center (DLR), Münchener Str. 20, 82234 Weßling, Germany

Key Points:

- We calculate the two-way radar attenuation on Enceladus considering a porous thermally insulating surface layer.
- For regions covered by a thick, insulating porous layer the detection of the ice-ocean interface is unlikely.
- For the same regions the high subsurface temperatures increase the likelihood that shallow brines are present and can be detected by radar.

Corresponding author: Wiliam Byrne, `William.Byrne@dlr.de`

Abstract

The presence of a global ocean, the water-rock interface at the base of the ocean, and the inferred ocean composition derived from sampling the active plume at the south pole of Enceladus, make Saturn's moon a promising location for habitable conditions in the Solar System. Due to its thin (<35 km) and cold ice shell, Enceladus is expected to exhibit favourable conditions for direct detection of the ice-ocean interface using low-frequency radar sounder instruments. Here we investigate the two-way radar attenuation in the Enceladus ice shell, focusing on the effect of a porous icy layer generated by Enceladus' jet activity. Our results show that as little as 2% of the ice shell can be penetrated in regions covered by thick and strongly insulating porous layers. However, the high subsurface temperatures in these regions could promote the formation of brines at shallow depth that can be detected by future radar measurements.

Plain Language Summary

Saturn's moon Enceladus is a prime target for planetary exploration and for the search of habitable conditions beyond Earth. Beneath its icy surface, this small moon is thought to harbor a global ocean, presumably sampled by active water jets which have been observed at Enceladus' south pole. Moreover, shallow brines may exist within the ice shell. The detection of subsurface water reservoirs (either the ocean or shallow brines) that can be achieved by radar is fundamental in characterizing Enceladus' subsurface environment and its habitability potential. In this study we calculate the attenuation of radar signals through the ice shell in the presence of snow deposits that are believed to exist on the surface of Enceladus due to its water jets activity. We find that the ice-ocean interface may not be reached in regions covered by thick snow deposits that act as a blanket and keep the subsurface warm. However, in these regions, due to the high subsurface temperatures, shallow water bodies are likely to exist and could be detected by future radar observations.

1 Introduction

Saturn's moon, Enceladus is considered a priority target for future planetary missions due to its high astrobiological potential (Choblet et al., 2021; Cable et al., 2021). Water jets presumably originating from a subsurface ocean have been observed at the south pole of Enceladus by NASA's Cassini mission (e..g., Porco et al., 2006; Hansen et al., 2006), and their analysis provides a direct window into the ocean composition (Postberg et al., 2009) that, in turn, can help to understand the nature and amount of impurities that may exist within the ice shell. The most direct access to the ice shell structure could be provided by future radar measurements. Radar instruments are widely used to characterize polar ice sheets on the Earth (e.g., Schroeder et al., 2020) and Mars (Plaut et al., 2007; Phillips et al., 2008), and are part of the instrument suites of JUICE and Europa Clipper to investigate the ice shells of icy moons in the Jupiter system (Bruzzone et al., 2013; Blankenship et al., 2009).

The ice shell thickness of Enceladus is thought to vary gradually depending on latitude and longitude (Čadek et al., 2019; Hemingway & Mittal, 2019). It is expected to be thinnest at the south-polar region and thickest at the equatorial sub- and anti-Saturn points. Depending on the chosen shape model (Nimmo et al., 2011; Tajeddine et al., 2017) and assumed density contrast between the ice shell and the ocean, ice shell thickness models suggest strong variations, with values as low as 5 km at the south pole and as high as 35 km in equatorial regions, or a more homogeneous ice shell thickness distribution with less than 15 km differences (Hemingway & Mittal, 2019).

Enceladus' jet activity likely leads to the formation of a highly porous layer at the top of the ice shell due to the material fall-back from the plume eruptions at the south pole (Kempf et al., 2010). If present, such a porous layer could be stable on most of Enceladus's surface due to the low temperatures (Gundlach et al., 2018). The thickness of this porous layer and its distribution are poorly constrained, but local thicknesses of up to 700 m have been reported from the analysis of pit chains on the surface of Enceladus (Martin et al., 2023). Such a thick porous layer may strongly affect the thermal state of the ice shell, leading to higher signal attenuation (Souček et al., 2023), but its effects have not been investigated so far.

Another aspect that can affect the subsurface temperature and hence the two-way attenuation is the way heat is currently transported through Enceladus's ice shell. Heat transport through the ice shell could occur either by conduction or by convection and can affect the thermal state of the ice shell with typically lower temperatures for a conductive scenario. Here we focus on conductive cases. This scenario is very likely given the thin ice shell (<35 km) and high viscosity at the conditions relevant for Enceladus's ice shell (Barr & McKinnon, 2007). High viscosities are expected based on the grain sizes observed in polar ice sheets on the Earth (between 1 and 5 mm, (Montagnat & Duval, 2000)) that are considered to be good analogues for the icy shells in the outer Solar System.

2 Methods

2.1 Thermal State of Enceladus's Ice Shell

To study how ice shell properties impact radar attenuation, we use 1-D steady-state, conductive thermal models of Enceladus's interior. The model is solved numerically using the stationary heat-conduction equation for a spherical shell with an outer radius R_{top} of 252 km and an inner radius R_{bot}, which is varied to account for surface fluctuations on Enceladus. The steady-state heat conduction equation reads:

$$\frac{1}{r^2}\frac{\partial}{\partial r}\left(kr^2\frac{\partial T}{\partial r}\right) = 0, \tag{1}$$

where r is the radius, k the thermal conductivity of ice, and T the temperature. The thermal conductivity of ice is temperature-dependent and follows the parametrization of Petrenko and Whitworth (1999):

$$k(T) = \frac{651}{T}. \tag{2}$$

We solve Eq. 1 numerically and use as boundary conditions the surface temperature of Enceladus at the top and the melting temperature of water-ice at the ice-ocean interface. For the surface temperature we use a value of 60 K, but additional tests with values of 70 and 85 K are shown in the Supplementary Information (Fig. S2.1)

In contrast to previous studies that calculated the two-way radar attenuation in icy shells, we consider the effects of a porous ice layer. On Enceladus, the main process responsible for the formation of such a layer is the deposition of material from the active plume at the south pole (Kempf et al., 2010; Southworth et al., 2019). This porous ice layer may considerably affect the thermal state of the ice shell due to its low thermal conductivity. Thermal conductivity values have been measured for porous icy layers in laboratory experiments (Seiferlin et al., 1996) and derived from thermophysical modeling (Ferrari et al., 2021). Such measurements have provided wide ranges in results (between 0.001 and 0.025 $\mathrm{W m^{-1} K^{-1}}$). Therefore, in order to cover a wide parameter space, we vary the thermal conductivity of this porous layer between 0.1 and 0.001 $\mathrm{W m^{-1} K^{-1}}$.

The thickness and spatial distribution of a porous icy layer on Enceladus is poorly constrained. A recent study by Martin et al. (2023) proposed porous layer thicknesses of up to 700 m (mean of 250 m) based on the analysis of tectonic pit chains. We test a variety of porous layer thicknesses up to 700 m and employ different spatial distributions to account for uncertainties related to the porous layer on Enceladus.

2.2 Radar Attenuation

Radar attenuation in ice is caused by dielectric absorption losses as well as scattering losses. A common assumption in low-frequency radar sounding is that scattering losses are negligible due to the long wavelengths with respect to the scattering structures (e.g., ice grains) within the ice. Hence, attenuation purely driven by absorption losses is assumed here. Following the work of Kalousová et al. (2017) and Souček et al. (2023), we calculate the two-way attenuation along the propagation path at depth d, which was subdivided into N layers, as:

$$A_2(d) = \sum_{i=0}^{N} 2A_1(d_i)\Delta d \tag{3}$$

where d_0 represents the surface layer, d_N is the final layer, $A_1(d_i)$ is the one-way attenuation at depth d_i, and Δd the thickness of each layer used in calculating A_1.

The one-way attenuation A_1 (in dB/km) of a radar signal is proportional to the electrical conductivity of ice (σ) within the range of High Frequency (HF) and Very High Frequency (VHF) (Matsuoka et al., 2012), and can be approximated as follows:

$$A_1 \approx 0.914\sigma. \tag{4}$$

The electrical conductivity of ice in terrestrial sounding experiments depends on the ice temperature along with the presence of chemical impurities within the ice, and can be written as follows (Corr et al., 1993):

$$\sigma = \sum_{i=0}^{1} \sigma_i^0 C_i \exp\left[-\frac{E_i}{k_B}\left(\frac{1}{T} - \frac{1}{T_r}\right)\right], \tag{5}$$

with each contribution representing one component that affects the electrical conductivity. Each summand requires the material molar electrical conductivity σ_i at reference temperature $T_r = 251\,\mathrm{K}$, molar concentration C_i, activation energy E_i, local ice temperature T, and the Boltzmann constant k_B. In this study we use the same values as in Table 1 of Souček et al. (2023). The index 0 indicates a scenario of a pure water-ice shell, while i = 1 adds the effects of the maximum theoretical chloride concentration in pure water-ice (Souček et al., 2023).

Similar to Kalousová et al. (2017) and Souček et al. (2023), we calculate the plausible attenuation ranges within Enceladus's ice shell. We use "low-loss" to indicate that the attenuation model considers only pure water ice, while the "hight-loss" model is characterized by a homogeneous mixture of pure water ice and 300 μM of chloride. The chloride concentration has been chosen based on plume material sampled during NASA's Cassini mission. Although carbonate salts, chloride, silica, and ammonia/ammonium have been detected, only chloride is expected to exist within the ice shell with significant concentrations (of up to 300 μM) to impact an orbital radar sounder (Souček et al., 2023).

3 Results

First, we investigate the difference between the "high" and "low" loss attenuation models in multiple 1-dimensional scenarios of Enceladus's internal structure. To this end, we calculate temperature profiles and corresponding two-way attenuation for various ice shell thicknesses, thicknesses of the porous layer, and porous layer thermal conductivities (Fig. 1).

We define a penetration depth, which is the depth at which the two-way attenuation reaches a 100 dB. The relative penetration depth is the penetration depth divided by the total ice shell thickness of the respective scenario. The relative penetration depth strongly depends on temperature, as the latter affects the electrical conductivity. For a

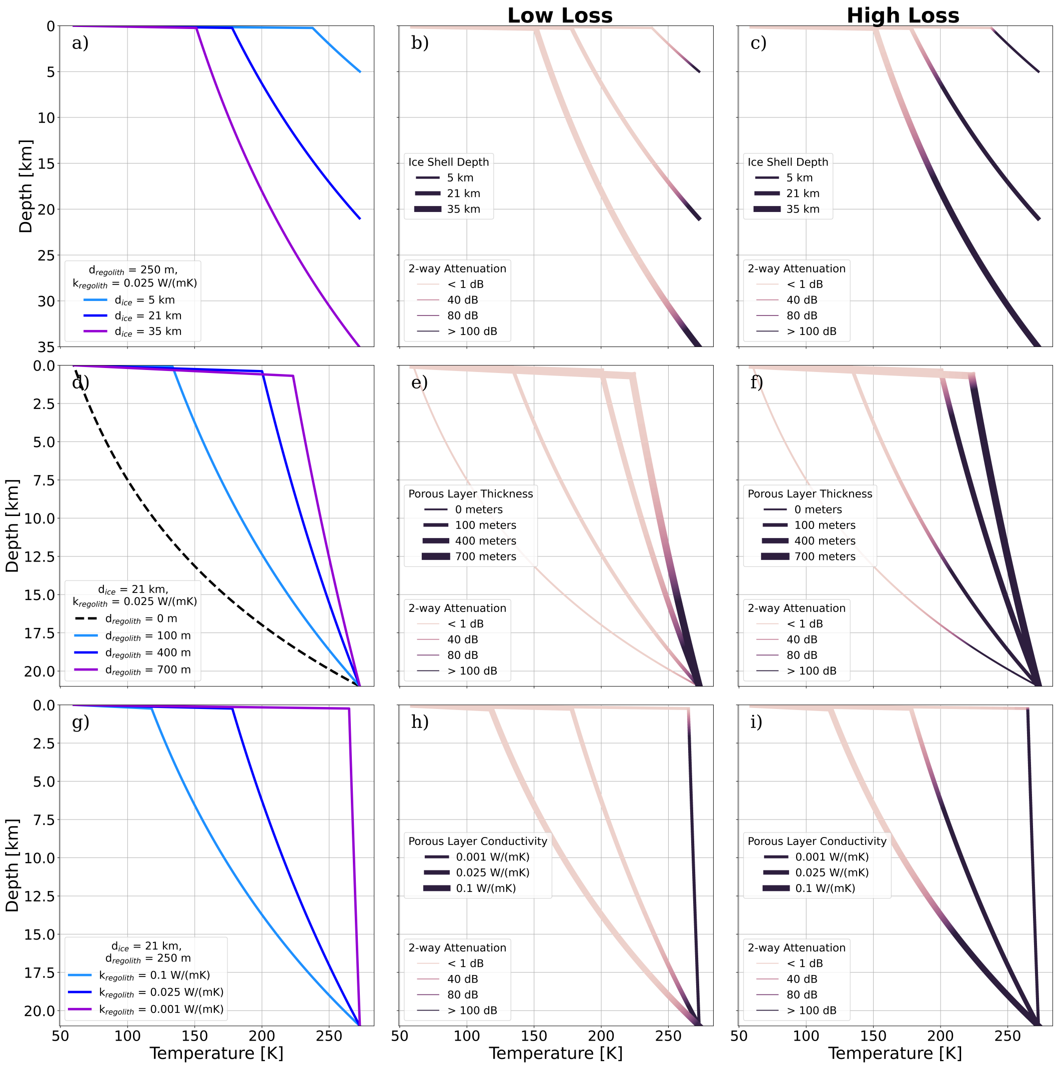

Figure 1. The two-way attenuation (A_2) for various: a) ice shell depths (5 – 35 km), b) porous layer thicknesses (0 – 700 m), and c) porous layer thermal conductivities (0.1 – 0.001 $\mathrm{Wm^{-1}K^{-1}}$). Panels d-f) show the low-loss scenarios, while panels g-i) show the high-loss cases.

conductive ice shell, the temperature itself depends on the thickness of the ice shell, and to a first order on the presence of a porous layer. The porous layer leads to a high thermal gradient near the surface due to its insulating effect caused by its low thermal conductivity. The relative penetration depth in a low-loss scenario is 91%, 94%, and 95%, for ice shell thicknesses of 5 km, 21 km, and 35 km, respectively. The penetration depths relative to the total depth in the hight-loss case are 16%, 33%, and 48%, for the same ice shell thicknesses of 5 km, 21 km, and 35 km, respectively.

We can clearly observe in Fig. 1 that the attenuation dramatically increases with increasing porous layer thickness. This can be again attributed to the insulating effect of the porous layer, an effect that becomes more pronounced with increasing porous layer thickness. As observed on Fig. 1d, the difference between the temperature profiles with and without a porous layer of 700 m is as large as 150 K at shallow depth. The low-loss scenario with no porous layer only reaches 53.4 dB at the ice-ocean interface, which was set here to 21 km. In the low-loss scenario, the presence of a 100 m porous layer increases the 2-way attenuation to 100 dB or higher at 99% of the ice shell depth. The relative penetration depth associated with the 100 dB limit is 88% for a 400 m and 74% for a 700 m porous layer. For the hight-loss scenario, the radar attenuation increases to more than 100 dB before reaching the ice-ocean interface even when no porous layer is considered. Thus, the relative penetration depth is 88% of the total ice shell for the no porous layer case, 64% for the 100 m porous layer case, 16% for the 400 m case, and 8% for the 700 m porous layer.

The thermal conductivity of the porous layer can significantly impact the thermal profile within the ice shell. A highly insulating porous layer (i.e., thermal conductivity of 0.001 $\mathrm{Wm^{-1}K^{-1}}$) with a thickness of 250 m, leads to a warm ice shell, only a few degrees colder than the ice-ocean interface. In the low-loss scenario, the 2-way attenuation for the case with the highest thermal conductivity of the porous layer (i.e., 0.1 $\mathrm{Wm^{-1}K^{-1}}$) reaches 95 dB at the ice-ocean interface. For a thermal conductivity of 0.025 $\mathrm{Wm^{-1}K^{-1}}$ of the porous layer, the 2-way attenuation reaches the 100 dB limit at about ∼80% of the ice shell in both high- and low-loss scenarios. In the case with the most insulating porous layer (i.e., regolith thermal conductivity of 0.001 $\mathrm{Wm^{-1}K^{-1}}$), the 2-way attenuation reaches 100 dB before 10% of the ice shell is penetrated in both the high and low-loss scenarios.

In Fig. 2 we explore a large set of parameter combinations. Each cell represents a single simulation (equivalent to one line graph in Fig. 1). The value inside each cell represents the relative penetration depth. The simulations cover ice shell thicknesses of 5 km, 21 km, and 35 km, as well as the low-loss and high-loss attenuation models.

None of the high-loss models reach 100% relative depth penetration, even with a 5 km ice shell with no porous layer. Most simulations using a highly insulating porous layer with a thermal conductivity of 0.001 $\mathrm{Wm^{-1}K^{-1}}$ reach less than 10% relative penetration depth. Of the total of 90 simulations, 16 models penetrate the whole ice shell, with those models generally having porous layers with small thicknesses and high thermal conductivities.

As expected, every combination of parameters has a lower relative penetration depth in the high-loss attenuation model compared to low-loss. Secondly, the relative penetration depth decreases with increasing porous layer thickness and decreasing thermal conductivity. However, a trend reversal occurs (i.e., penetration depth increases) in highly insulating porous layers (apart from the the 35 km low-loss scenarios). Such a reversal only occurs in scenarios with both a highly conductive and very deep porous layer. This behavior can be explained by the fact that with increasing porous layer thickness, the thermal state of the ice shell starts to approach that of a conductive ice shell characterized by a single thermal conductivity. If the porous layer makes up the entire ice shell,

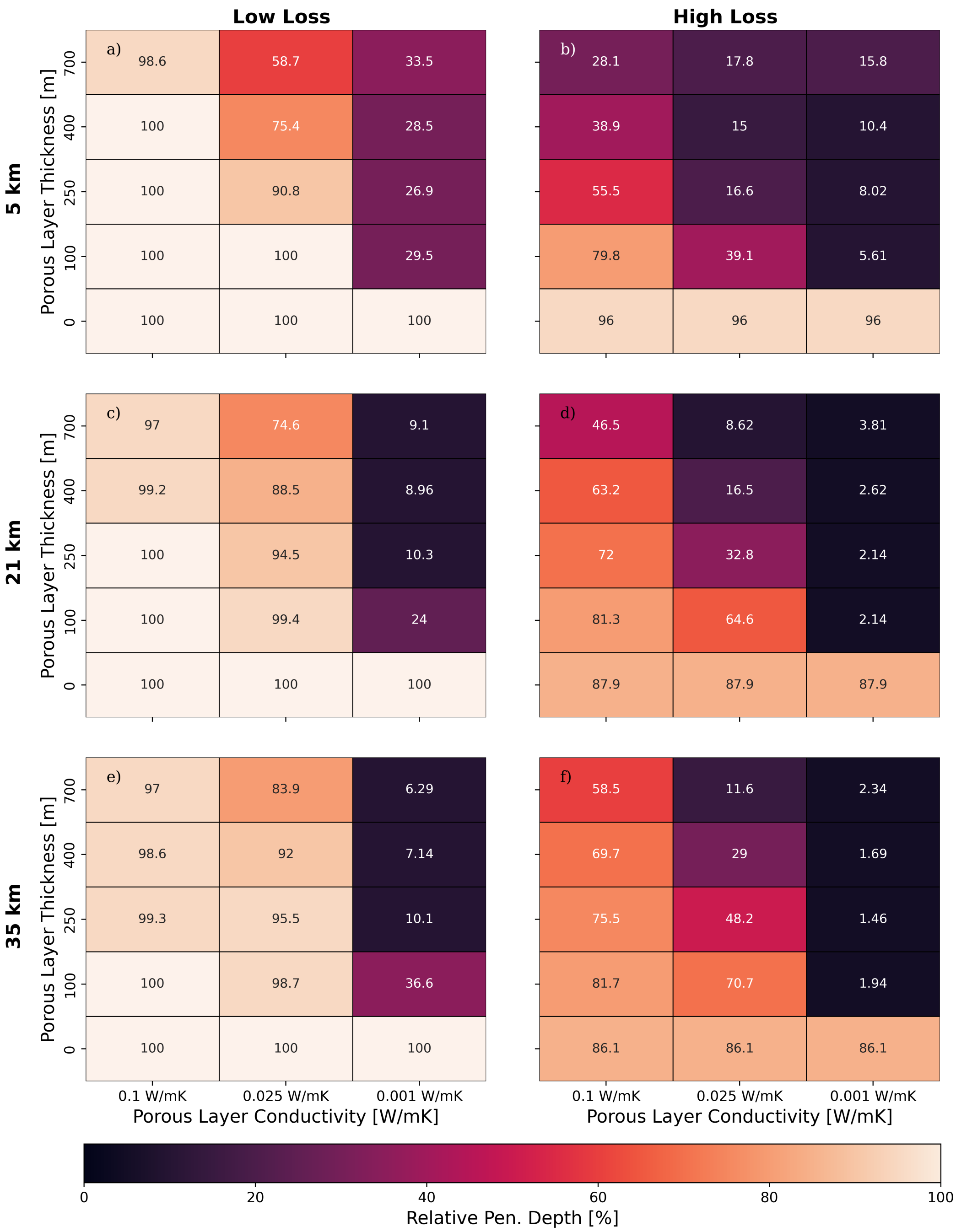

Figure 2. The relative penetration depth of a radar signal for ice shell thicknesses of 5 km (a, d), 21 km (b, e), and 35 km (c, f) and various porous layer thicknesses and thermal conductivities for low-loss (left column) and high-loss (right column) scenarios.

the steady-state thermal state will be similar to that of a homogeneous ice shell with a thermal conductivity of pure water-ice.

Beyond 1-D analysis, we generate attenuation maps (Fig. 3 a)) using a global ice shell thickness map from Hemingway and Mittal (2019), based on a shape model of Nimmo et al. (2011), gravitational data, and assuming a density contrast between the ice shell and the subsurface ocean of 95 $\mathrm{kg\,m^{-3}}$ similar to some of the models of (Hemingway & Mittal, 2019). Additional attenuation maps using a different ice shell thickness, shape model and ice-ocean density contrast are available in the Supporting Information (SI), Section S3.

The attenuation was calculated by treating each data point as a single temperature profile using the corresponding ice shell thickness at the respective location. We constructed two distribution models for the porous layer under the assumption that the thickness of the porous layer varies only with latitude and: 1) exponentially decreases from a 700-m-thick layer at the south pole to 10-m-thick layer at the north pole of Enceladus, which we denote as the "exponential-global distribution" (Fig. 3 b) while 2) the porous layer is absent within the 5° of the south pole and then exponentially decreases from 255 m to 0 m at equator (Fig. 3 c), which we will call "exponential-hemispheric distribution". In all cases the conductivity of the porous layer is 0.025 $\mathrm{Wm^{-1}K^{-1}}$.

In the low-loss attenuation maps (Fig. 3 d, e, and f), a majority of the surface has more than 90% relative penetration depth, with both the no-porous-layer and the exponential-hemispheric distribution cases having 100% global radar penetration down to the ice-ocean interface. In all three high-loss scenarios, we observe a small band of 100% relative penetration depth roughly 5° in latitude away from the south pole. The thin ice shell at the south pole allows for the signal to reach the ice-ocean interface even in the presence of a thick porous layer (i.e., 700 m in the exponential-global distribution case).

We note that in all cases besides the high-loss exponential-global distribution case, the penetration depth reaches more than 80% of the ice shell for most locations.

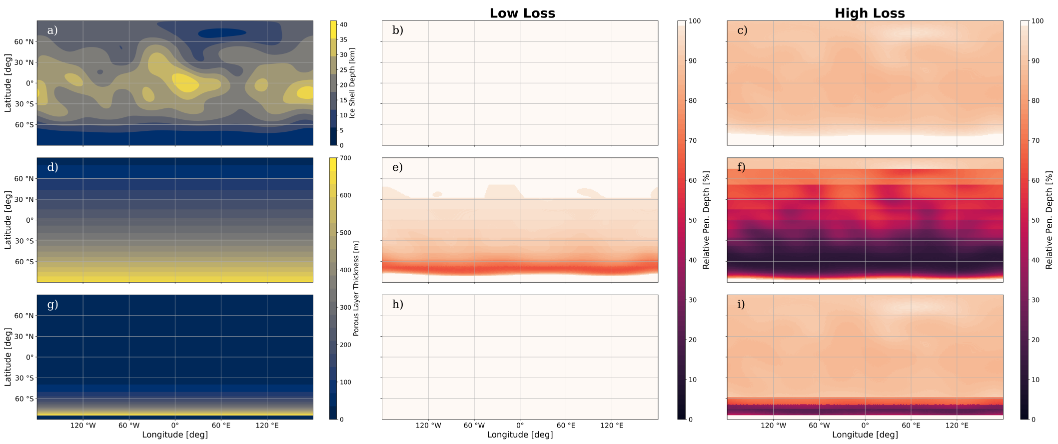

Figure 3. Maps of the: a) ice shell thickness (Hemingway & Mittal, 2019) and porous layer distribution for b) the "exponential-global scenario" and c) the "exponential-hemispheric scenario" (see text). The radar penetration depth relative to the ice shell thickness in panel a) is shown for d) no porous layer, e) exponential-global and f) exponential-hemispheric distribution of the porous layer. Panels g), h) and i) show the high-loss cases.

In Fig. 4, we calculate the two-way attenuation at the eutectic interfaces of ammonium chloride and ammonia following Souček et al. (2023) for the exponential-hemispheric distribution of the porous layer (i.e., exponential decrease from 255 m at 85°S to 0 m at equator) and assuming a thermal conductivity of the porous layer of 0.025 $\mathrm{W m^{-1} K^{-1}}$.

The eutectic interface of ammonium chloride (NH_4Cl) is defined by the 257.79 K isotherm, while the one for ammonia (NH_3) by the 175.45 K isotherm (Marion et al., 2012). Panels a and b of Fig. 4 show the depths at which the eutectic of NH_3 and NH_4Cl, respectively, are reached. Fig. 4 c and d show the two-way attenuation for the low-loss attenuation models, while the values obtained for the high-loss cases are shown in Fig. 4 e and f. Additional maps including different ice shell thicknesses and porous layer distribution are available in the SI (Section S4).

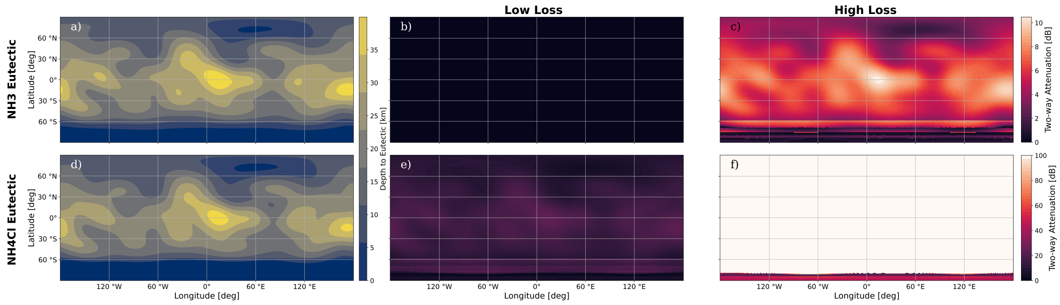

Figure 4. Maps showing the depth of: a) ammonia (NH_3) and b) ammonium chloride (NH_4Cl) eutectic interface for the exponential-hemispheric distribution of the porous layer. Panels c) and d) indicate the corresponding two-way attenuation values for the low-loss case at the eutectic interface of NH_3 and NH_4Cl, respectively. Panels e) and f) are similar to c) and d), but for the high-loss scenarios.

The difference between the average depth of the ice-ocean interface and the average depth of the NH_4Cl eutectic interface is only 700 m. This is due to the fact that the temperature of the NH_4Cl eutectic interface is only 20 K lower than the melting temperature of water-ice at the base of the ice shell shown in Fig. 4 a. In contrast, the difference between the average depth of the ammonia eutectic interface and that of the ice-ocean interface is 5 km, as NH_3 has a much lower eutectic temperature of only 175.45 K. Given the low eutectic temperature of NH_3, the two-way attenuation for the low-loss case (Fig. 4 c) does not exceed 0.1 dB. For the eutectic interface of NH_4Cl, the two-way attenuation shows an average value 13.7 dB in the low-loss scenario (Fig. 4 d). In the high-loss attenuation case, the two-way attenuation at the eutectic interface of NH_3 is only $\sim$5 dB (Fig. 4 e), while at the eutectic interface of NH_4Cl the average two-way attenuation is about 400 dB (Fig. 4 f).

4 Discussion

Similar to other studies (Kalousová et al., 2017; Souček et al., 2023), we assume a threshold of 100 dB for the two-way radar attenuation, above which the radar instrument would no longer be able to detect subsurface interfaces. However, we note that this threshold is only an estimate, that might change in a mission scenario depending on the instrument design, operation scenarios, as well as surface and subsurface characteristics (see e.g., Kalousová et al., 2017; Benedikter et al., 2024)[for a detailed discussion]. Our tests show that varying the two-way attenuation limit between 70 and 130 dB would not significantly impact the results presented in Fig. 2. In these cases we observe a difference to the relative penetration depth shown in Fig. 2 of up to only 10% (see Fig. S1.1–S1.2 in the SI).

On Enceladus, the surface temperature lies between 60 and 85 K, the latter values being representative for the south polar region (Spencer et al., 2006). We tested the effects of a higher surface temperature (i.e., 85 K) on out calculated radar attenuation values (Fig. S2.1). A higher surface temperature shifts the ice shell temperature to higher values and leads to a smaller relative penetration depth. However the differences between using a surface temperature of 85 K compared to 60 K are only of the order of 2 – 4%.

We note that our study assumes simple distributions of a porous layer on Enceladus to give a first order overview of the potential detection of the ice-ocean interface via radar sounding. While our results show that the ice-ocean interface will be challenging to detect in particular in regions covered by thick and highly thermal insulating porous layers, we note that large uncertainties exist for the global spatial distribution of such a porous layer on Enceladus. While models of the distribution of a porous layer on Enceladus exist (Kempf et al., 2010; Southworth et al., 2019), they typically investigate only the generation of such a layer through plume deposition. Such models indicate that tectonized regions on the leading and trailing hemispheres receive the least amount of material deposition, but that the plume eruption style (i.e., curtain-like vs. jet-like) affects the amount of snow deposits in the northern hemisphere (Southworth et al., 2019). The predicted distribution of a material deposition from models of jet-style eruptions seem to be consistent with the distribution of pit chains on the surface of Enceladus. The latter, however, can only give a lower bound for the thickness of the porous layer, as the pits do not necessarily need to reach the base of the layer (Martin et al., 2023).

Another important factor that will affect the thermal state of the ice shell and hence the two-way attenuation is the thermal conductivity of the porous layer. A recent study by Jabaud et al. (2024) investigated the mechanical properties of powder-like materials similar to the expected snow deposits on Enceladus that are also suggested to exist to some extent on Europa. This study concluded that on Enceladus, the lower gravity leads to higher cohesion and the formation of loose, highly porous material. A high porosity is directly linked to a low thermal conductivity and thus highly insulating behavior. As shown in this study, an insulating porous layer would increase the ice shell temperature such that the resulting temperature contrast between the base of the porous layer and the ocean may be only 10s of degrees K. Such high average temperatures could result in the formation of shallow brines that could provide a radar-detectable source (Souček et al., 2023). Our models show that even in the presence of thick porous layers, the two-way radar attenuation remains below 25 dB for eutectic interfaces of NH_3 and NH_4Cl in the low-loss scenario. In the high-loss cases, only the NH_4Cl interface lies above the 100 dB threshold for most of the ice shell apart from within about 5° of the south pole. As these eutectic interfaces are defined by isotherms, their detection would provide valuable information about the thermal state of the ice shell and may help reconstructing not only the ice shell thickness (see discussion in Souček et al., 2023) but also the thickness of the porous layer that strongly affects the temperature in the ice shell and hence the depth of these interfaces.

This study has focused on the effect of a porous layer on two-way attenuation in a conductive ice shell. Future studies will test how such a porous layer, its thickness and spatial distribution, affects the ice shell dynamics and in particular the two-way radar attenuation for hot upwellings and cold downwellings. Depending on the ice shell temperature, cold downwellings could represent locations where the radar attenuation is low enough such that the ice-ocean interface may be reached, as previously discussed for Europa (Kalousová et al., 2017).

5 Conclusions

In this study we showed that a porous layer built up by the deposition of material from Enceladus's south pole plume or generated by impacts has a first order effect on the two-way radar attenuation. This porous layer acts as an insulation layer leading to high sub-surface temperatures and thus two-way attenuation. Through systematic parameter variations, we provide an extensive overview of the effects of a porous layer on the ability to reach the ice-ocean as well as other interfaces within the ice shell that are thought to exist based on the inferred ice shell chemistry.

Our investigations show that radar sounder instruments may penetrate anywhere from a few hundred meters to the entire ice shell of Enceladus. Nevertheless, those scenarios that prevent radar signals from reaching the ice ocean interface can provide valuable information about the ice shell. Identifying aspects of the Enceladus system that could prevent ocean detection may prove fundamental in further characterizing icy worlds. Valuable insights may be gained, such as the existence of near-surface liquid reservoirs, which are very likely for cases with high salt content and a porous layer on top that keeps the interior comparatively warm. Such brine reservoirs are considered niches for life, and their potential to be directly accessible by future missions is much greater compared to that of the subsurface oceans.

6 Open Research

Additional calculations including different ice shell thicknesses are available in the Supplementary Information. All data used in the figures and the code necessary to reproduce the calculations are available on Zenodo (Byrne et al., 2024)

Acknowledgments

ACP and TRB acknowledge funding from the Deutsche Forschungsgemeinschaft (DFG, German Research Foundation) – Project-ID 460819306. AB and HH were supperted in part by the European Space Agency (ESA) under Contract 4000141148/23/NL/KK/ov. We thank Douglas Hemingway for providing the ice thickness maps from Hemingway and Mittal (2019). We thank Gregor Steinbrügge and Dustin Schroeder for insightful discussions on radar attenuation on icy moons.

References

Barr, A. C., & McKinnon, W. B. (2007). Convection in Enceladus' ice shell: Conditions for initiation. *Geophysical Research Letters*, *34*(9).

Benedikter, A., Matar, J., Masaki, N., Otto, T., Hussmann, H., Perihar, T., ... Imbembo, E. (2024). A Fractionated Radar Sounder Concept for Subsurface Exploration of Saturn's Icy Moon Enceladus. In *Eusar 2024* (p. a261).

Blankenship, D. D., Young, D. A., Moore, W. B., & Moore, J. C. (2009). Radar sounding of Europa's subsurface properties and processes: The view from Earth. *Europa*, 631–654.

Bruzzone, L., Plaut, J. J., Alberti, G., Blankenship, D. D., Bovolo, F., Campbell, B. A., ... others (2013). RIME: Radar for icy moon exploration. In *2013 ieee international geoscience and remote sensing symposium-igarss* (pp. 3907–3910).

Byrne, W., Plesa, A.-C., Rückriemen-Bez, T., Hussmann, H., & Benedikter, A. (2024, June). *Radar Attenuation for Subsurface Sounding on Enceladus: Effects of a Porous Ice Layer* [Dataset]. Zenodo. Retrieved from `https://doi.org/10.5281/zenodo.10932227` doi: 10.5281/zenodo.10932227

Cable, M. L., Porco, C., Glein, C. R., German, C. R., MacKenzie, S. M., Neveu, M., ... others (2021). The science case for a return to Enceladus. *The planetary* *science journal*, *2*(4), 132.

Čadek, O., Souček, O., & Běhounková, M. (2019). Is Airy isostasy applicable to icy moons? *Geophysical Research Letters*, *46*(24), 14299–14306.

Choblet, G., Tobie, G., Buch, A., Čadek, O., Barge, L. M., Bēhounková, M., ... others (2021). Enceladus as a potential oasis for life: Science goals and investigations for future explorations. *Experimental Astronomy*, 1–39.

Corr, H., Moore, J. C., & Nicholls, K. W. (1993). Radar absorption due to impurities in Antarctic ice. *Geophysical Research Letters*, *20*(11), 1071–1074.

Ferrari, C., Lucas, A., & Jacquemoud, S. (2021). The thermal emission of Saturn's icy moons-Effects of topography and regolith properties. *Astronomy & Astrophysics*, *655*, A8.

Gundlach, B., Ratte, J., Blum, J., Oesert, J., & Gorb, S. (2018). Sintering and sublimation of micrometre-sized water-ice particles: The formation of surface crusts on icy Solar System bodies. *Monthly Notices of the Royal Astronomical Society*, *479*(4), 5272–5287.

Hansen, C. J., Esposito, L., Stewart, A., Colwell, J., Hendrix, A., Pryor, W., ... West, R. (2006). Enceladus' water vapor plume. *Science*, *311*(5766), 1422–1425.

Hemingway, D. J., & Mittal, T. (2019). Enceladus's ice shell structure as a window on internal heat production. *Icarus*, *332*, 111–131.

Jabaud, B., Artoni, R., Tobie, G., Le Menn, E., & Richard, P. (2024). Cohesive properties of ice powders analogous to fresh plume deposits on Enceladus and Europa. *Icarus*, *409*, 115859.

Kalousová, K., Schroeder, D. M., & Soderlund, K. M. (2017). Radar attenuation in Europa's ice shell: Obstacles and opportunities for constraining the shell thickness and its thermal structure. *Journal of Geophysical Research: Planets*, *122*(3), 524–545.

Kempf, S., Beckmann, U., & Schmidt, J. (2010). How the Enceladus dust plume feeds Saturn's E ring. *Icarus*, *206*(2), 446–457.

Marion, G., Kargel, J., Catling, D., & Lunine, J. (2012). Modeling ammonia–ammonium aqueous chemistries in the Solar System's icy bodies. *Icarus*, *220*(2), 932–946.

Martin, E. S., Whitten, J. L., Kattenhorn, S. A., Collins, G. C., Southworth, B. S., Wiser, L. S., & Prindle, S. (2023). Measurements of regolith thicknesses on Enceladus: Uncovering the record of plume activity. *Icarus*, *392*, 115369.

Matsuoka, K., MacGregor, J. A., & Pattyn, F. (2012). Predicting radar attenuation within the Antarctic ice sheet. *Earth and Planetary Science Letters*, *359*, 173–183.

Montagnat, M., & Duval, P. (2000). Rate controlling processes in the creep of polar ice, influence of grain boundary migration associated with recrystallization. *Earth and Planetary Science Letters*, *183*(1-2), 179–186.

Nimmo, F., Bills, B., & Thomas, P. (2011). Geophysical implications of the long-wavelength topography of the Saturnian satellites. *Journal of Geophysical Research: Planets*, *116*(E11).

Petrenko, V. F., & Whitworth, R. W. (1999). *Physics of ice.* OUP Oxford.

Phillips, R. J., Zuber, M. T., Smrekar, S. E., Mellon, M. T., Head, J. W., Tanaka, K. L., ... Marinangeli, L. (2008). Mars north polar deposits: Stratigraphy, age, and geodynamical response. *Science*, *320*(5880), 1182–1185. doi: 10.1126/science.1157546

Plaut, J. J., Picardi, G., Safaeinili, A., Ivanov, A. B., Milkovich, S. M., Cicchetti, A., ... others (2007). Subsurface radar sounding of the south polar layered deposits of Mars. *science*, *316*(5821), 92–95.

Porco, C. C., Helfenstein, P., Thomas, P., Ingersoll, A., Wisdom, J., West, R., ... others (2006). Cassini observes the active south pole of Enceladus. *science*, *311*(5766), 1393–1401.

Postberg, F., Kempf, S., Schmidt, J., Brilliantov, N., Beinsen, A., Abel, B., … Srama, R. (2009). Sodium salts in E-ring ice grains from an ocean below the surface of Enceladus. *Nature*, *459*(7250), 1098–1101.

Schroeder, D. M., Bingham, R. G., Blankenship, D. D., Christianson, K., Eisen, O., Flowers, G. E., … Siegert, M. J. (2020). Five decades of radioglaciology. *Annals of Glaciology*, *61*(81), 1–13.

Seiferlin, K., Kömle, N., Kargl, G., & Spohn, T. (1996). Line heat-source measurements of the thermal conductivity of porous H2O ice, CO2 ice and mineral powders under space conditions. *Planetary and Space Science*, *44*(7), 691–704.

Souček, O., Běhounková, M., Schroeder, D. M., Wolfenbarger, N. S., Kalousová, K., Steinbrügge, G., & Soderlund, K. M. (2023). Radar Attenuation in Enceladus' Ice Shell: Obstacles and Opportunities for Constraining Shell Thickness, Chemistry, and Thermal Structure. *Journal of Geophysical Research: Planets*, *128*(2), e2022JE007626.

Southworth, B. S., Kempf, S., & Spitale, J. (2019). Surface deposition of the Enceladus plume and the zenith angle of emissions. *Icarus*, *319*, 33–42.

Spencer, J., Pearl, J., Segura, M., Flasar, F., Mamoutkine, A., Romani, P., … Lopes, R. (2006). Cassini encounters Enceladus: Background and the discovery of a south polar hot spot. *science*, *311*(5766), 1401–1405.

Tajeddine, R., Soderlund, K. M., Thomas, P. C., Helfenstein, P., Hedman, M. M., Burns, J. A., & Schenk, P. M. (2017). True polar wander of Enceladus from topographic data. *Icarus*, *295*, 46–60.

Radar Attenuation for Subsurface Sounding on Enceladus: Effects of a Porous Ice Layer

William Byrne[1,2], Ana-Catalina Plesa[1], Tina Rückriemen-Bez[1], Hauke Hussmann[1], Andreas Benedikter[3]

[1]Institute of Planetary Research, German Aerospace Center (DLR), Rutherford Str. 2, 12489 Berlin, Germany
[2]University of Maryland, College Park, MD 20742, USA
[3]Microwaves and Radar Institute, German Aerospace Center (DLR), Münchener Str. 20, 82234 Weßling, Germany

Key Points:

- We calculate the two-way radar attenuation on Enceladus considering a porous thermally insulating surface layer.
- For regions covered by a thick, insulating porous layer the detection of the ice-ocean interface is unlikely.
- For the same regions the high subsurface temperatures increase the likelihood that shallow brines are present and can be detected by radar.

Corresponding author: Wiliam Byrne, `William.Byrne@dlr.de`

Abstract

The presence of a global ocean, the water-rock interface at the base of the ocean, and the inferred ocean composition derived from sampling the active plume at the south pole of Enceladus, make Saturn's moon a promising location for habitable conditions in the Solar System. Due to its thin (<35 km) and cold ice shell, Enceladus is expected to exhibit favourable conditions for direct detection of the ice-ocean interface using low-frequency radar sounder instruments. Here we investigate the two-way radar attenuation in the Enceladus ice shell, focusing on the effect of a porous icy layer generated by Enceladus' jet activity. Our results show that as little as 2% of the ice shell can be penetrated in regions covered by thick and strongly insulating porous layers. However, the high subsurface temperatures in these regions could promote the formation of brines at shallow depth that can be detected by future radar measurements.

Plain Language Summary

Saturn's moon Enceladus is a prime target for planetary exploration and for the search of habitable conditions beyond Earth. Beneath its icy surface, this small moon is thought to harbor a global ocean, presumably sampled by active water jets which have been observed at Enceladus' south pole. Moreover, shallow brines may exist within the ice shell. The detection of subsurface water reservoirs (either the ocean or shallow brines) that can be achieved by radar is fundamental in characterizing Enceladus' subsurface environment and its habitability potential. In this study we calculate the attenuation of radar signals through the ice shell in the presence of snow deposits that are believed to exist on the surface of Enceladus due to its water jets activity. We find that the ice-ocean interface may not be reached in regions covered by thick snow deposits that act as a blanket and keep the subsurface warm. However, in these regions, due to the high subsurface temperatures, shallow water bodies are likely to exist and could be detected by future radar observations.

1 Introduction

Saturn's moon, Enceladus is considered a priority target for future planetary missions due to its high astrobiological potential (Choblet et al., 2021; Cable et al., 2021). Water jets presumably originating from a subsurface ocean have been observed at the south pole of Enceladus by NASA's Cassini mission (e..g., Porco et al., 2006; Hansen et al., 2006), and their analysis provides a direct window into the ocean composition (Postberg et al., 2009) that, in turn, can help to understand the nature and amount of impurities that may exist within the ice shell. The most direct access to the ice shell structure could be provided by future radar measurements. Radar instruments are widely used to characterize polar ice sheets on the Earth (e.g., Schroeder et al., 2020) and Mars (Plaut et al., 2007; Phillips et al., 2008), and are part of the instrument suites of JUICE and Europa Clipper to investigate the ice shells of icy moons in the Jupiter system (Bruzzone et al., 2013; Blankenship et al., 2009).

The ice shell thickness of Enceladus is thought to vary gradually depending on latitude and longitude (Čadek et al., 2019; Hemingway & Mittal, 2019). It is expected to be thinnest at the south-polar region and thickest at the equatorial sub- and anti-Saturn points. Depending on the chosen shape model (Nimmo et al., 2011; Tajeddine et al., 2017) and assumed density contrast between the ice shell and the ocean, ice shell thickness models suggest strong variations, with values as low as 5 km at the south pole and as high as 35 km in equatorial regions, or a more homogeneous ice shell thickness distribution with less than 15 km differences (Hemingway & Mittal, 2019).

Enceladus' jet activity likely leads to the formation of a highly porous layer at the top of the ice shell due to the material fall-back from the plume eruptions at the south pole (Kempf et al., 2010). If present, such a porous layer could be stable on most of Enceladus's surface due to the low temperatures (Gundlach et al., 2018). The thickness of this porous layer and its distribution are poorly constrained, but local thicknesses of up to 700 m have been reported from the analysis of pit chains on the surface of Enceladus (Martin et al., 2023). Such a thick porous layer may strongly affect the thermal state of the ice shell, leading to higher signal attenuation (Souček et al., 2023), but its effects have not been investigated so far.

Another aspect that can affect the subsurface temperature and hence the two-way attenuation is the way heat is currently transported through Enceladus's ice shell. Heat transport through the ice shell could occur either by conduction or by convection and can affect the thermal state of the ice shell with typically lower temperatures for a conductive scenario. Here we focus on conductive cases. This scenario is very likely given the thin ice shell (<35 km) and high viscosity at the conditions relevant for Enceladus's ice shell (Barr & McKinnon, 2007). High viscosities are expected based on the grain sizes observed in polar ice sheets on the Earth (between 1 and 5 mm, (Montagnat & Duval, 2000)) that are considered to be good analogues for the icy shells in the outer Solar System.

2 Methods

2.1 Thermal State of Enceladus's Ice Shell

To study how ice shell properties impact radar attenuation, we use 1-D steady-state, conductive thermal models of Enceladus's interior. The model is solved numerically using the stationary heat-conduction equation for a spherical shell with an outer radius R_{top} of 252 km and an inner radius R_{bot}, which is varied to account for surface fluctuations on Enceladus. The steady-state heat conduction equation reads:

$$\frac{1}{r^2}\frac{\partial}{\partial r}\left(kr^2\frac{\partial T}{\partial r}\right) = 0, \tag{1}$$

where r is the radius, k the thermal conductivity of ice, and T the temperature. The thermal conductivity of ice is temperature-dependent and follows the parametrization of Petrenko and Whitworth (1999):

$$k(T) = \frac{651}{T}. \tag{2}$$

We solve Eq. 1 numerically and use as boundary conditions the surface temperature of Enceladus at the top and the melting temperature of water-ice at the ice-ocean interface. For the surface temperature we use a value of 60 K, but additional tests with values of 70 and 85 K are shown in the Supplementary Information (Fig. S2.1)

In contrast to previous studies that calculated the two-way radar attenuation in icy shells, we consider the effects of a porous ice layer. On Enceladus, the main process responsible for the formation of such a layer is the deposition of material from the active plume at the south pole (Kempf et al., 2010; Southworth et al., 2019). This porous ice layer may considerably affect the thermal state of the ice shell due to its low thermal conductivity. Thermal conductivity values have been measured for porous icy layers in laboratory experiments (Seiferlin et al., 1996) and derived from thermophysical modeling (Ferrari et al., 2021). Such measurements have provided wide ranges in results (between 0.001 and 0.025 $\mathrm{W m^{-1} K^{-1}}$). Therefore, in order to cover a wide parameter space, we vary the thermal conductivity of this porous layer between 0.1 and 0.001 $\mathrm{W m^{-1} K^{-1}}$.

The thickness and spatial distribution of a porous icy layer on Enceladus is poorly constrained. A recent study by Martin et al. (2023) proposed porous layer thicknesses of up to 700 m (mean of 250 m) based on the analysis of tectonic pit chains. We test a variety of porous layer thicknesses up to 700 m and employ different spatial distributions to account for uncertainties related to the porous layer on Enceladus.

2.2 Radar Attenuation

Radar attenuation in ice is caused by dielectric absorption losses as well as scattering losses. A common assumption in low-frequency radar sounding is that scattering losses are negligible due to the long wavelengths with respect to the scattering structures (e.g., ice grains) within the ice. Hence, attenuation purely driven by absorption losses is assumed here. Following the work of Kalousová et al. (2017) and Souček et al. (2023), we calculate the two-way attenuation along the propagation path at depth d, which was subdivided into N layers, as:

$$A_2(d) = \sum_{i=0}^{N} 2A_1(d_i)\Delta d \tag{3}$$

where d_0 represents the surface layer, d_N is the final layer, $A_1(d_i)$ is the one-way attenuation at depth d_i, and Δd the thickness of each layer used in calculating A_1.

The one-way attenuation A_1 (in dB/km) of a radar signal is proportional to the electrical conductivity of ice (σ) within the range of High Frequency (HF) and Very High Frequency (VHF) (Matsuoka et al., 2012), and can be approximated as follows:

$$A_1 \approx 0.914\sigma. \tag{4}$$

The electrical conductivity of ice in terrestrial sounding experiments depends on the ice temperature along with the presence of chemical impurities within the ice, and can be written as follows (Corr et al., 1993):

$$\sigma = \sum_{i=0}^{1} \sigma_i^0 C_i \exp\left[-\frac{E_i}{k_B}\left(\frac{1}{T} - \frac{1}{T_r}\right)\right], \tag{5}$$

with each contribution representing one component that affects the electrical conductivity. Each summand requires the material molar electrical conductivity σ_i at reference temperature $T_r = 251\,\mathrm{K}$, molar concentration C_i, activation energy E_i, local ice temperature T, and the Boltzmann constant k_B. In this study we use the same values as in Table 1 of Souček et al. (2023). The index 0 indicates a scenario of a pure water-ice shell, while i = 1 adds the effects of the maximum theoretical chloride concentration in pure water-ice (Souček et al., 2023).

Similar to Kalousová et al. (2017) and Souček et al. (2023), we calculate the plausible attenuation ranges within Enceladus's ice shell. We use "low-loss" to indicate that the attenuation model considers only pure water ice, while the "hight-loss" model is characterized by a homogeneous mixture of pure water ice and 300 μM of chloride. The chloride concentration has been chosen based on plume material sampled during NASA's Cassini mission. Although carbonate salts, chloride, silica, and ammonia/ammonium have been detected, only chloride is expected to exist within the ice shell with significant concentrations (of up to 300 μM) to impact an orbital radar sounder (Souček et al., 2023).

3 Results

First, we investigate the difference between the "high" and "low" loss attenuation models in multiple 1-dimensional scenarios of Enceladus's internal structure. To this end, we calculate temperature profiles and corresponding two-way attenuation for various ice shell thicknesses, thicknesses of the porous layer, and porous layer thermal conductivities (Fig. 1).

We define a penetration depth, which is the depth at which the two-way attenuation reaches a 100 dB. The relative penetration depth is the penetration depth divided by the total ice shell thickness of the respective scenario. The relative penetration depth strongly depends on temperature, as the latter affects the electrical conductivity. For a

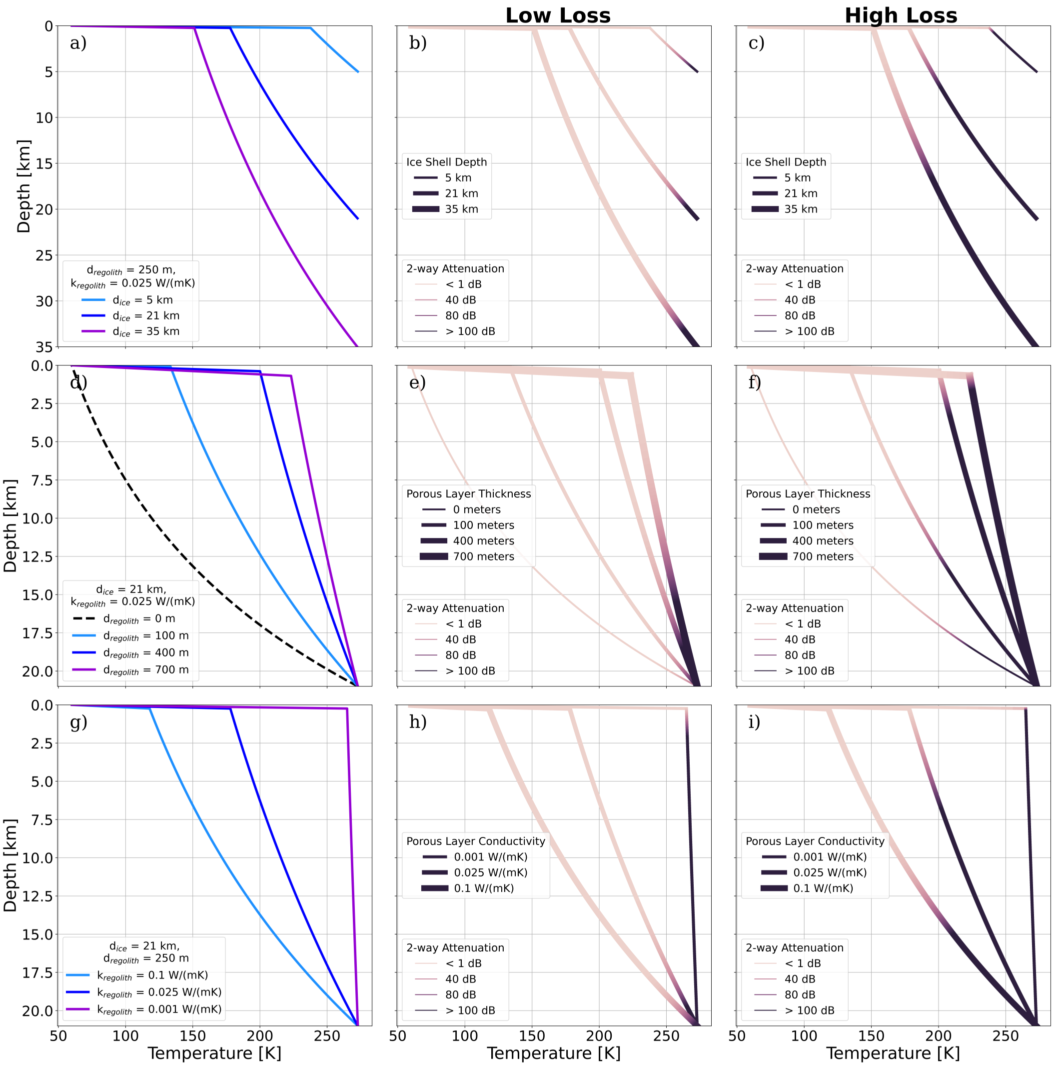

Figure 1. The two-way attenuation (A_2) for various: a) ice shell depths (5 – 35 km), b) porous layer thicknesses (0 – 700 m), and c) porous layer thermal conductivities (0.1 – 0.001 $\mathrm{Wm^{-1}K^{-1}}$). Panels d-f) show the low-loss scenarios, while panels g-i) show the high-loss cases.

conductive ice shell, the temperature itself depends on the thickness of the ice shell, and to a first order on the presence of a porous layer. The porous layer leads to a high thermal gradient near the surface due to its insulating effect caused by its low thermal conductivity. The relative penetration depth in a low-loss scenario is 91%, 94%, and 95%, for ice shell thicknesses of 5 km, 21 km, and 35 km, respectively. The penetration depths relative to the total depth in the hight-loss case are 16%, 33%, and 48%, for the same ice shell thicknesses of 5 km, 21 km, and 35 km, respectively.

We can clearly observe in Fig. 1 that the attenuation dramatically increases with increasing porous layer thickness. This can be again attributed to the insulating effect of the porous layer, an effect that becomes more pronounced with increasing porous layer thickness. As observed on Fig. 1d, the difference between the temperature profiles with and without a porous layer of 700 m is as large as 150 K at shallow depth. The low-loss scenario with no porous layer only reaches 53.4 dB at the ice-ocean interface, which was set here to 21 km. In the low-loss scenario, the presence of a 100 m porous layer increases the 2-way attenuation to 100 dB or higher at 99% of the ice shell depth. The relative penetration depth associated with the 100 dB limit is 88% for a 400 m and 74% for a 700 m porous layer. For the hight-loss scenario, the radar attenuation increases to more than 100 dB before reaching the ice-ocean interface even when no porous layer is considered. Thus, the relative penetration depth is 88% of the total ice shell for the no porous layer case, 64% for the 100 m porous layer case, 16% for the 400 m case, and 8% for the 700 m porous layer.

The thermal conductivity of the porous layer can significantly impact the thermal profile within the ice shell. A highly insulating porous layer (i.e., thermal conductivity of 0.001 $\mathrm{Wm^{-1}K^{-1}}$) with a thickness of 250 m, leads to a warm ice shell, only a few degrees colder than the ice-ocean interface. In the low-loss scenario, the 2-way attenuation for the case with the highest thermal conductivity of the porous layer (i.e., 0.1 $\mathrm{Wm^{-1}K^{-1}}$) reaches 95 dB at the ice-ocean interface. For a thermal conductivity of 0.025 $\mathrm{Wm^{-1}K^{-1}}$ of the porous layer, the 2-way attenuation reaches the 100 dB limit at about $\sim$80% of the ice shell in both high- and low-loss scenarios. In the case with the most insulating porous layer (i.e., regolith thermal conductivity of 0.001 $\mathrm{Wm^{-1}K^{-1}}$), the 2-way attenuation reaches 100 dB before 10% of the ice shell is penetrated in both the high and low-loss scenarios.

In Fig. 2 we explore a large set of parameter combinations. Each cell represents a single simulation (equivalent to one line graph in Fig. 1). The value inside each cell represents the relative penetration depth. The simulations cover ice shell thicknesses of 5 km, 21 km, and 35 km, as well as the low-loss and high-loss attenuation models.

None of the high-loss models reach 100% relative depth penetration, even with a 5 km ice shell with no porous layer. Most simulations using a highly insulating porous layer with a thermal conductivity of 0.001 $\mathrm{Wm^{-1}K^{-1}}$ reach less than 10% relative penetration depth. Of the total of 90 simulations, 16 models penetrate the whole ice shell, with those models generally having porous layers with small thicknesses and high thermal conductivities.

As expected, every combination of parameters has a lower relative penetration depth in the high-loss attenuation model compared to low-loss. Secondly, the relative penetration depth decreases with increasing porous layer thickness and decreasing thermal conductivity. However, a trend reversal occurs (i.e., penetration depth increases) in highly insulating porous layers (apart from the the 35 km low-loss scenarios). Such a reversal only occurs in scenarios with both a highly conductive and very deep porous layer. This behavior can be explained by the fact that with increasing porous layer thickness, the thermal state of the ice shell starts to approach that of a conductive ice shell characterized by a single thermal conductivity. If the porous layer makes up the entire ice shell,

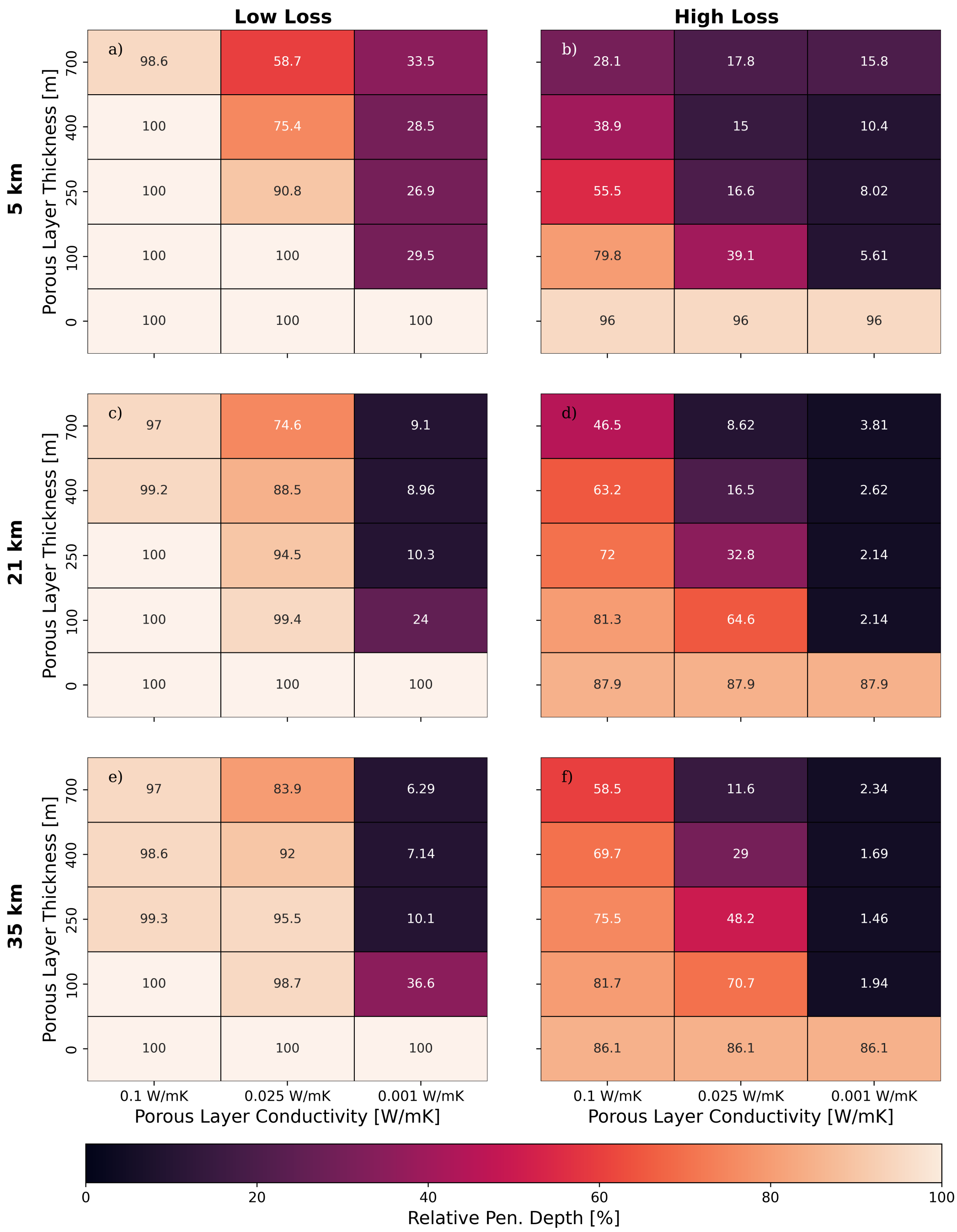

Figure 2. The relative penetration depth of a radar signal for ice shell thicknesses of 5 km (a, d), 21 km (b, e), and 35 km (c, f) and various porous layer thicknesses and thermal conductivities for low-loss (left column) and high-loss (right column) scenarios.

the steady-state thermal state will be similar to that of a homogeneous ice shell with a thermal conductivity of pure water-ice.

Beyond 1-D analysis, we generate attenuation maps (Fig. 3 a)) using a global ice shell thickness map from Hemingway and Mittal (2019), based on a shape model of Nimmo et al. (2011), gravitational data, and assuming a density contrast between the ice shell and the subsurface ocean of $95\,\mathrm{kg\,m^{-3}}$ similar to some of the models of (Hemingway & Mittal, 2019). Additional attenuation maps using a different ice shell thickness, shape model and ice-ocean density contrast are available in the Supporting Information (SI), Section S3.

The attenuation was calculated by treating each data point as a single temperature profile using the corresponding ice shell thickness at the respective location. We constructed two distribution models for the porous layer under the assumption that the thickness of the porous layer varies only with latitude and: 1) exponentially decreases from a 700-m-thick layer at the south pole to 10-m-thick layer at the north pole of Enceladus, which we denote as the "exponential-global distribution" (Fig. 3 b) while 2) the porous layer is absent within the 5° of the south pole and then exponentially decreases from 255 m to 0 m at equator (Fig. 3 c), which we will call "exponential-hemispheric distribution". In all cases the conductivity of the porous layer is $0.025\,\mathrm{Wm^{-1}K^{-1}}$.

In the low-loss attenuation maps (Fig. 3 d, e, and f), a majority of the surface has more than 90% relative penetration depth, with both the no-porous-layer and the exponential-hemispheric distribution cases having 100% global radar penetration down to the ice-ocean interface. In all three high-loss scenarios, we observe a small band of 100% relative penetration depth roughly 5° in latitude away from the south pole. The thin ice shell at the south pole allows for the signal to reach the ice-ocean interface even in the presence of a thick porous layer (i.e., 700 m in the exponential-global distribution case).

We note that in all cases besides the high-loss exponential-global distribution case, the penetration depth reaches more than 80% of the ice shell for most locations.

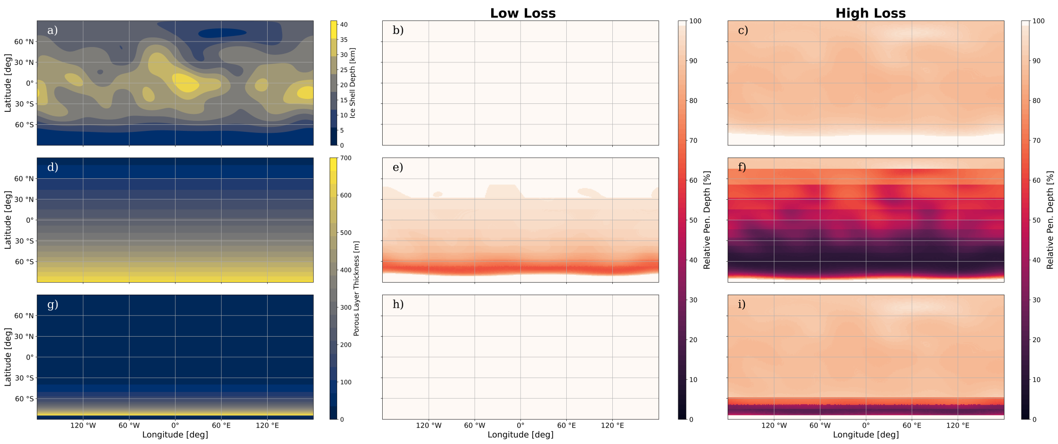

Figure 3. Maps of the: a) ice shell thickness (Hemingway & Mittal, 2019) and porous layer distribution for b) the "exponential-global scenario" and c) the "exponential-hemispheric scenario" (see text). The radar penetration depth relative to the ice shell thickness in panel a) is shown for d) no porous layer, e) exponential-global and f) exponential-hemispheric distribution of the porous layer. Panels g), h) and i) show the high-loss cases.

In Fig. 4, we calculate the two-way attenuation at the eutectic interfaces of ammonium chloride and ammonia following Souček et al. (2023) for the exponential-hemispheric distribution of the porous layer (i.e., exponential decrease from 255 m at 85°S to 0 m at equator) and assuming a thermal conductivity of the porous layer of 0.025 $\mathrm{W m^{-1} K^{-1}}$.

The eutectic interface of ammonium chloride (NH_4Cl) is defined by the 257.79 K isotherm, while the one for ammonia (NH_3) by the 175.45 K isotherm (Marion et al., 2012). Panels a and b of Fig. 4 show the depths at which the eutectic of NH_3 and NH_4Cl, respectively, are reached. Fig. 4 c and d show the two-way attenuation for the low-loss attenuation models, while the values obtained for the high-loss cases are shown in Fig. 4 e and f. Additional maps including different ice shell thicknesses and porous layer distribution are available in the SI (Section S4).

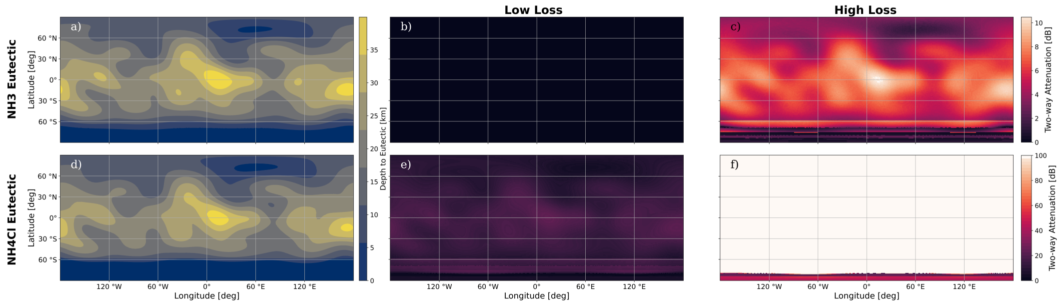

Figure 4. Maps showing the depth of: a) ammonia (NH_3) and b) ammonium chloride (NH_4Cl) eutectic interface for the exponential-hemispheric distribution of the porous layer. Panels c) and d) indicate the corresponding two-way attenuation values for the low-loss case at the eutectic interface of NH_3 and NH_4Cl, respectively. Panels e) and f) are similar to c) and d), but for the high-loss scenarios.

The difference between the average depth of the ice-ocean interface and the average depth of the NH_4Cl eutectic interface is only 700 m. This is due to the fact that the temperature of the NH_4Cl eutectic interface is only 20 K lower than the melting temperature of water-ice at the base of the ice shell shown in Fig. 4 a. In contrast, the difference between the average depth of the ammonia eutectic interface and that of the ice-ocean interface is 5 km, as NH_3 has a much lower eutectic temperature of only 175.45 K. Given the low eutectic temperature of NH_3, the two-way attenuation for the low-loss case (Fig. 4 c) does not exceed 0.1 dB. For the eutectic interface of NH_4Cl, the two-way attenuation shows an average value 13.7 dB in the low-loss scenario (Fig. 4 d). In the high-loss attenuation case, the two-way attenuation at the eutectic interface of NH_3 is only $\sim$5 dB (Fig. 4 e), while at the eutectic interface of NH_4Cl the average two-way attenuation is about 400 dB (Fig. 4 f).

4 Discussion

Similar to other studies (Kalousová et al., 2017; Souček et al., 2023), we assume a threshold of 100 dB for the two-way radar attenuation, above which the radar instrument would no longer be able to detect subsurface interfaces. However, we note that this threshold is only an estimate, that might change in a mission scenario depending on the instrument design, operation scenarios, as well as surface and subsurface characteristics (see e.g., Kalousová et al., 2017; Benedikter et al., 2024)[for a detailed discussion]. Our tests show that varying the two-way attenuation limit between 70 and 130 dB would not significantly impact the results presented in Fig. 2. In these cases we observe a difference to the relative penetration depth shown in Fig. 2 of up to only 10% (see Fig. S1.1–S1.2 in the SI).

On Enceladus, the surface temperature lies between 60 and 85 K, the latter values being representative for the south polar region (Spencer et al., 2006). We tested the effects of a higher surface temperature (i.e., 85 K) on out calculated radar attenuation values (Fig. S2.1). A higher surface temperature shifts the ice shell temperature to higher values and leads to a smaller relative penetration depth. However the differences between using a surface temperature of 85 K compared to 60 K are only of the order of 2 – 4%.

We note that our study assumes simple distributions of a porous layer on Enceladus to give a first order overview of the potential detection of the ice-ocean interface via radar sounding. While our results show that the ice-ocean interface will be challenging to detect in particular in regions covered by thick and highly thermal insulating porous layers, we note that large uncertainties exist for the global spatial distribution of such a porous layer on Enceladus. While models of the distribution of a porous layer on Enceladus exist (Kempf et al., 2010; Southworth et al., 2019), they typically investigate only the generation of such a layer through plume deposition. Such models indicate that tectonized regions on the leading and trailing hemispheres receive the least amount of material deposition, but that the plume eruption style (i.e., curtain-like vs. jet-like) affects the amount of snow deposits in the northern hemisphere (Southworth et al., 2019). The predicted distribution of a material deposition from models of jet-style eruptions seem to be consistent with the distribution of pit chains on the surface of Enceladus. The latter, however, can only give a lower bound for the thickness of the porous layer, as the pits do not necessarily need to reach the base of the layer (Martin et al., 2023).

Another important factor that will affect the thermal state of the ice shell and hence the two-way attenuation is the thermal conductivity of the porous layer. A recent study by Jabaud et al. (2024) investigated the mechanical properties of powder-like materials similar to the expected snow deposits on Enceladus that are also suggested to exist to some extent on Europa. This study concluded that on Enceladus, the lower gravity leads to higher cohesion and the formation of loose, highly porous material. A high porosity is directly linked to a low thermal conductivity and thus highly insulating behavior. As shown in this study, an insulating porous layer would increase the ice shell temperature such that the resulting temperature contrast between the base of the porous layer and the ocean may be only 10s of degrees K. Such high average temperatures could result in the formation of shallow brines that could provide a radar-detectable source (Souček et al., 2023). Our models show that even in the presence of thick porous layers, the two-way radar attenuation remains below 25 dB for eutectic interfaces of NH_3 and NH_4Cl in the low-loss scenario. In the high-loss cases, only the NH_4Cl interface lies above the 100 dB threshold for most of the ice shell apart from within about 5° of the south pole. As these eutectic interfaces are defined by isotherms, their detection would provide valuable information about the thermal state of the ice shell and may help reconstructing not only the ice shell thickness (see discussion in Souček et al., 2023) but also the thickness of the porous layer that strongly affects the temperature in the ice shell and hence the depth of these interfaces.

This study has focused on the effect of a porous layer on two-way attenuation in a conductive ice shell. Future studies will test how such a porous layer, its thickness and spatial distribution, affects the ice shell dynamics and in particular the two-way radar attenuation for hot upwellings and cold downwellings. Depending on the ice shell temperature, cold downwellings could represent locations where the radar attenuation is low enough such that the ice-ocean interface may be reached, as previously discussed for Europa (Kalousová et al., 2017).

5 Conclusions

In this study we showed that a porous layer built up by the deposition of material from Enceladus's south pole plume or generated by impacts has a first order effect on the two-way radar attenuation. This porous layer acts as an insulation layer leading to high sub-surface temperatures and thus two-way attenuation. Through systematic parameter variations, we provide an extensive overview of the effects of a porous layer on the ability to reach the ice-ocean as well as other interfaces within the ice shell that are thought to exist based on the inferred ice shell chemistry.

Our investigations show that radar sounder instruments may penetrate anywhere from a few hundred meters to the entire ice shell of Enceladus. Nevertheless, those scenarios that prevent radar signals from reaching the ice ocean interface can provide valuable information about the ice shell. Identifying aspects of the Enceladus system that could prevent ocean detection may prove fundamental in further characterizing icy worlds. Valuable insights may be gained, such as the existence of near-surface liquid reservoirs, which are very likely for cases with high salt content and a porous layer on top that keeps the interior comparatively warm. Such brine reservoirs are considered niches for life, and their potential to be directly accessible by future missions is much greater compared to that of the subsurface oceans.

6 Open Research

Additional calculations including different ice shell thicknesses are available in the Supplementary Information. All data used in the figures and the code necessary to reproduce the calculations are available on Zenodo (Byrne et al., 2024)

Acknowledgments

ACP and TRB acknowledge funding from the Deutsche Forschungsgemeinschaft (DFG, German Research Foundation) – Project-ID 460819306. AB and HH were supperted in part by the European Space Agency (ESA) under Contract 4000141148/23/NL/KK/ov. We thank Douglas Hemingway for providing the ice thickness maps from Hemingway and Mittal (2019). We thank Gregor Steinbrügge and Dustin Schroeder for insightful discussions on radar attenuation on icy moons.

References

Barr, A. C., & McKinnon, W. B. (2007). Convection in Enceladus' ice shell: Conditions for initiation. *Geophysical Research Letters*, *34*(9).

Benedikter, A., Matar, J., Masaki, N., Otto, T., Hussmann, H., Perihar, T., ... Imbembo, E. (2024). A Fractionated Radar Sounder Concept for Subsurface Exploration of Saturn's Icy Moon Enceladus. In *Eusar 2024* (p. a261).

Blankenship, D. D., Young, D. A., Moore, W. B., & Moore, J. C. (2009). Radar sounding of Europa's subsurface properties and processes: The view from Earth. *Europa*, 631–654.

Bruzzone, L., Plaut, J. J., Alberti, G., Blankenship, D. D., Bovolo, F., Campbell, B. A., ... others (2013). RIME: Radar for icy moon exploration. In *2013 ieee international geoscience and remote sensing symposium-igarss* (pp. 3907–3910).

Byrne, W., Plesa, A.-C., Rückriemen-Bez, T., Hussmann, H., & Benedikter, A. (2024, June). *Radar Attenuation for Subsurface Sounding on Enceladus: Effects of a Porous Ice Layer* [Dataset]. Zenodo. Retrieved from `https://doi.org/10.5281/zenodo.10932227` doi: 10.5281/zenodo.10932227

Cable, M. L., Porco, C., Glein, C. R., German, C. R., MacKenzie, S. M., Neveu, M., ... others (2021). The science case for a return to Enceladus. *The planetary*

science journal, *2*(4), 132.
Čadek, O., Souček, O., & Běhounková, M. (2019). Is Airy isostasy applicable to icy moons? *Geophysical Research Letters*, *46*(24), 14299–14306.
Choblet, G., Tobie, G., Buch, A., Čadek, O., Barge, L. M., Bēhounková, M., … others (2021). Enceladus as a potential oasis for life: Science goals and investigations for future explorations. *Experimental Astronomy*, 1–39.
Corr, H., Moore, J. C., & Nicholls, K. W. (1993). Radar absorption due to impurities in Antarctic ice. *Geophysical Research Letters*, *20*(11), 1071–1074.
Ferrari, C., Lucas, A., & Jacquemoud, S. (2021). The thermal emission of Saturn's icy moons-Effects of topography and regolith properties. *Astronomy & Astrophysics*, *655*, A8.
Gundlach, B., Ratte, J., Blum, J., Oesert, J., & Gorb, S. (2018). Sintering and sublimation of micrometre-sized water-ice particles: The formation of surface crusts on icy Solar System bodies. *Monthly Notices of the Royal Astronomical Society*, *479*(4), 5272–5287.
Hansen, C. J., Esposito, L., Stewart, A., Colwell, J., Hendrix, A., Pryor, W., … West, R. (2006). Enceladus' water vapor plume. *Science*, *311*(5766), 1422–1425.
Hemingway, D. J., & Mittal, T. (2019). Enceladus's ice shell structure as a window on internal heat production. *Icarus*, *332*, 111–131.
Jabaud, B., Artoni, R., Tobie, G., Le Menn, E., & Richard, P. (2024). Cohesive properties of ice powders analogous to fresh plume deposits on Enceladus and Europa. *Icarus*, *409*, 115859.
Kalousová, K., Schroeder, D. M., & Soderlund, K. M. (2017). Radar attenuation in Europa's ice shell: Obstacles and opportunities for constraining the shell thickness and its thermal structure. *Journal of Geophysical Research: Planets*, *122*(3), 524–545.
Kempf, S., Beckmann, U., & Schmidt, J. (2010). How the Enceladus dust plume feeds Saturn's E ring. *Icarus*, *206*(2), 446–457.
Marion, G., Kargel, J., Catling, D., & Lunine, J. (2012). Modeling ammonia–ammonium aqueous chemistries in the Solar System's icy bodies. *Icarus*, *220*(2), 932–946.
Martin, E. S., Whitten, J. L., Kattenhorn, S. A., Collins, G. C., Southworth, B. S., Wiser, L. S., & Prindle, S. (2023). Measurements of regolith thicknesses on Enceladus: Uncovering the record of plume activity. *Icarus*, *392*, 115369.
Matsuoka, K., MacGregor, J. A., & Pattyn, F. (2012). Predicting radar attenuation within the Antarctic ice sheet. *Earth and Planetary Science Letters*, *359*, 173–183.
Montagnat, M., & Duval, P. (2000). Rate controlling processes in the creep of polar ice, influence of grain boundary migration associated with recrystallization. *Earth and Planetary Science Letters*, *183*(1-2), 179–186.
Nimmo, F., Bills, B., & Thomas, P. (2011). Geophysical implications of the long-wavelength topography of the Saturnian satellites. *Journal of Geophysical Research: Planets*, *116*(E11).
Petrenko, V. F., & Whitworth, R. W. (1999). *Physics of ice.* OUP Oxford.
Phillips, R. J., Zuber, M. T., Smrekar, S. E., Mellon, M. T., Head, J. W., Tanaka, K. L., … Marinangeli, L. (2008). Mars north polar deposits: Stratigraphy, age, and geodynamical response. *Science*, *320*(5880), 1182–1185. doi: 10.1126/science.1157546
Plaut, J. J., Picardi, G., Safaeinili, A., Ivanov, A. B., Milkovich, S. M., Cicchetti, A., … others (2007). Subsurface radar sounding of the south polar layered deposits of Mars. *science*, *316*(5821), 92–95.
Porco, C. C., Helfenstein, P., Thomas, P., Ingersoll, A., Wisdom, J., West, R., … others (2006). Cassini observes the active south pole of Enceladus. *science*, *311*(5766), 1393–1401.

Postberg, F., Kempf, S., Schmidt, J., Brilliantov, N., Beinsen, A., Abel, B., … Srama, R. (2009). Sodium salts in E-ring ice grains from an ocean below the surface of Enceladus. *Nature*, *459*(7250), 1098–1101.

Schroeder, D. M., Bingham, R. G., Blankenship, D. D., Christianson, K., Eisen, O., Flowers, G. E., … Siegert, M. J. (2020). Five decades of radioglaciology. *Annals of Glaciology*, *61*(81), 1–13.

Seiferlin, K., Kömle, N., Kargl, G., & Spohn, T. (1996). Line heat-source measurements of the thermal conductivity of porous H2O ice, CO2 ice and mineral powders under space conditions. *Planetary and Space Science*, *44*(7), 691–704.

Souček, O., Běhounková, M., Schroeder, D. M., Wolfenbarger, N. S., Kalousová, K., Steinbrügge, G., & Soderlund, K. M. (2023). Radar Attenuation in Enceladus' Ice Shell: Obstacles and Opportunities for Constraining Shell Thickness, Chemistry, and Thermal Structure. *Journal of Geophysical Research: Planets*, *128*(2), e2022JE007626.

Southworth, B. S., Kempf, S., & Spitale, J. (2019). Surface deposition of the Enceladus plume and the zenith angle of emissions. *Icarus*, *319*, 33–42.

Spencer, J., Pearl, J., Segura, M., Flasar, F., Mamoutkine, A., Romani, P., … Lopes, R. (2006). Cassini encounters Enceladus: Background and the discovery of a south polar hot spot. *science*, *311*(5766), 1401–1405.

Tajeddine, R., Soderlund, K. M., Thomas, P. C., Helfenstein, P., Hedman, M. M., Burns, J. A., & Schenk, P. M. (2017). True polar wander of Enceladus from topographic data. *Icarus*, *295*, 46–60.

Geophysical Research Letters

Supporting Information for

Radar Attenuation for Subsurface Sounding on Enceladus: Effects of a Porous Ice Layer

W. Byrne[1,2], A.-C. Plesa[1], T. Rückriemen-Bez[1], H. Hussmann[1], A. Benedikter[1]

[1]German Aerospace Center (DLR), Berlin, Germany., [2]University of Maryland, College Park, MD 20742, USA., [3]Microwaves and Radar Institute, German Aerospace Center (DLR), Münchener Str. 20, 82234 Weßling, Germany.

Contents of this file

Additional Supporting Information (Files uploaded separately)

1. Additional data sets and python scripts available on Zenodo repository

Introduction

In this supplementary information we present additional calculations to those discussed in the main manuscript of ”Radar Attenuation for Subsurface Sounding on Enceladus: Effects of a Porous Ice Layer”. In section S1 we show the effects of using a threshold of 70 dB and 130 dB for the two-way radar attenuation, above which the radar signal will not be able to detect subsurface interfaces. As a comparison, Fig. 2 in the main manuscript uses a threshold of 100 dB (*Kalousová et al.*, 2017; *Souček et al.*, 2023). In section S3 we calculate the relative penetration depth of the two-way radar attenuation for a different ice shell thickness model that uses the shape model of *Tajeddine et al.* (2017), an ice density of 900 kg m^{-3}, and an ocean density of 1100 kg m^{-3} that lead to more subtle ice shell thickness variations compared to the map in Fig. 3 of the main manuscript. Section S4 shows the depth of the ammonia and ammonium chloride eutectic interfaces similar the Fig. 4 of the main manuscript, but using an ”exponential-global distribution” of the porous ice layer.

S1 Two-way attenuation threshold

Here we performed sensitivity tests for the relative penetration depth of the two-way radar attenuation. Using the same set of models as discussed in Fig. 2 of the main manuscript, we computed the relative penetration depth of the two-way radar attenuation by assuming a 30% lower and higher threshold than the 100 dB value typically used in literature (*Kalousová et al.*, 2017; *Souček et al.*, 2023). Our models show that a thershold of 70 dB (Fig. 1.1) or 130 dB (Fig. 1.2) would only change the relative penetration depth by at most 10% compared to the results obtained when using a threshold value of 100 dB.

S2 Surface temperature effects

In this section, we test the effects of a higher surface temperature on the two-way radar attenuation, since on Enceladus the surface temperature varies between 60 and 85 K according to the data collected by the Cassini Composite Infrared Spectrometer (CIRS) (*Spencer et al.*, 2006). To this end, we used a surface temperature of 85 K (Fig. 2.1). When compared to Fig. 2 of the main manuscript, our results show that the a higher surface temperature (85 K instead of 60 K) leads to at most 2 – 4 % decrease in the relative penetration depth.

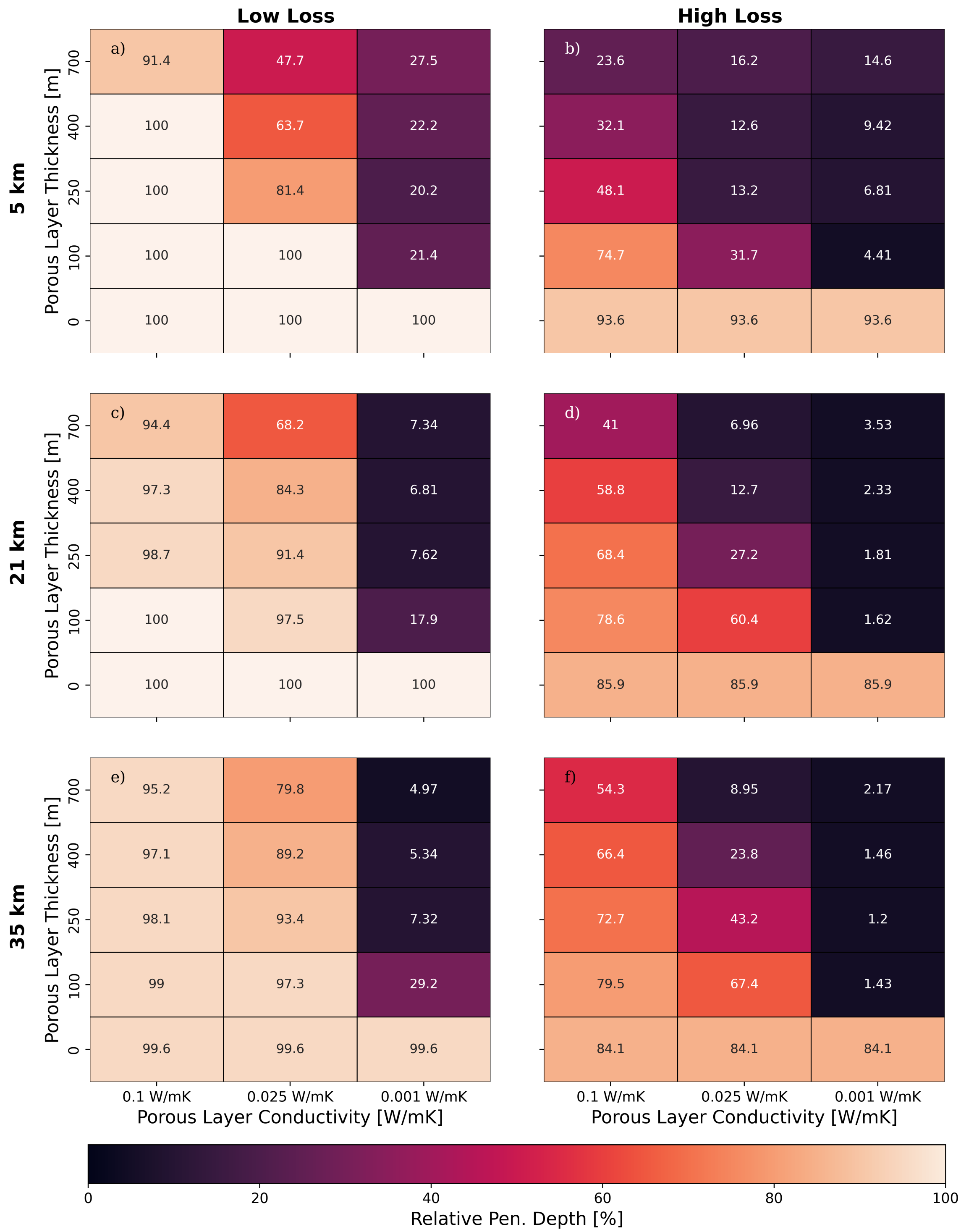

Figure 1.1: Systematic investigation of the relative penetration depth of a radar signal for ice shell thicknesses of 5 km (a, d), 21 km (b, e), and 35 km (c, f) and various porous thicknesses and thermal conductivities for low loss (left column) and high loss (right column) scenarios using a threshold for the two-way radar attenuation of 70 dB.

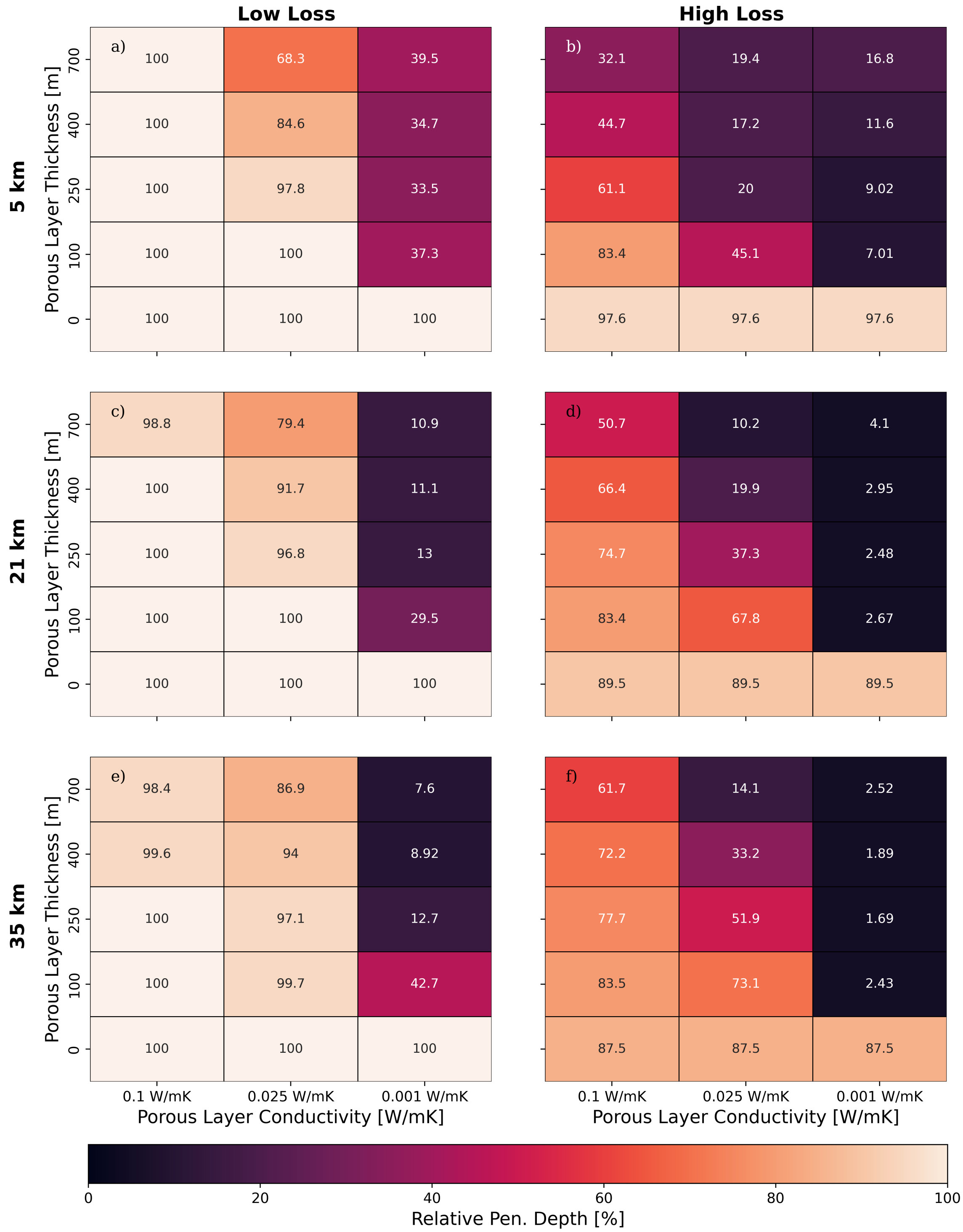

Figure 1.2: Similar as Fig. 1.1, but using a threshold for the two-way radar attenuation of 130 dB.

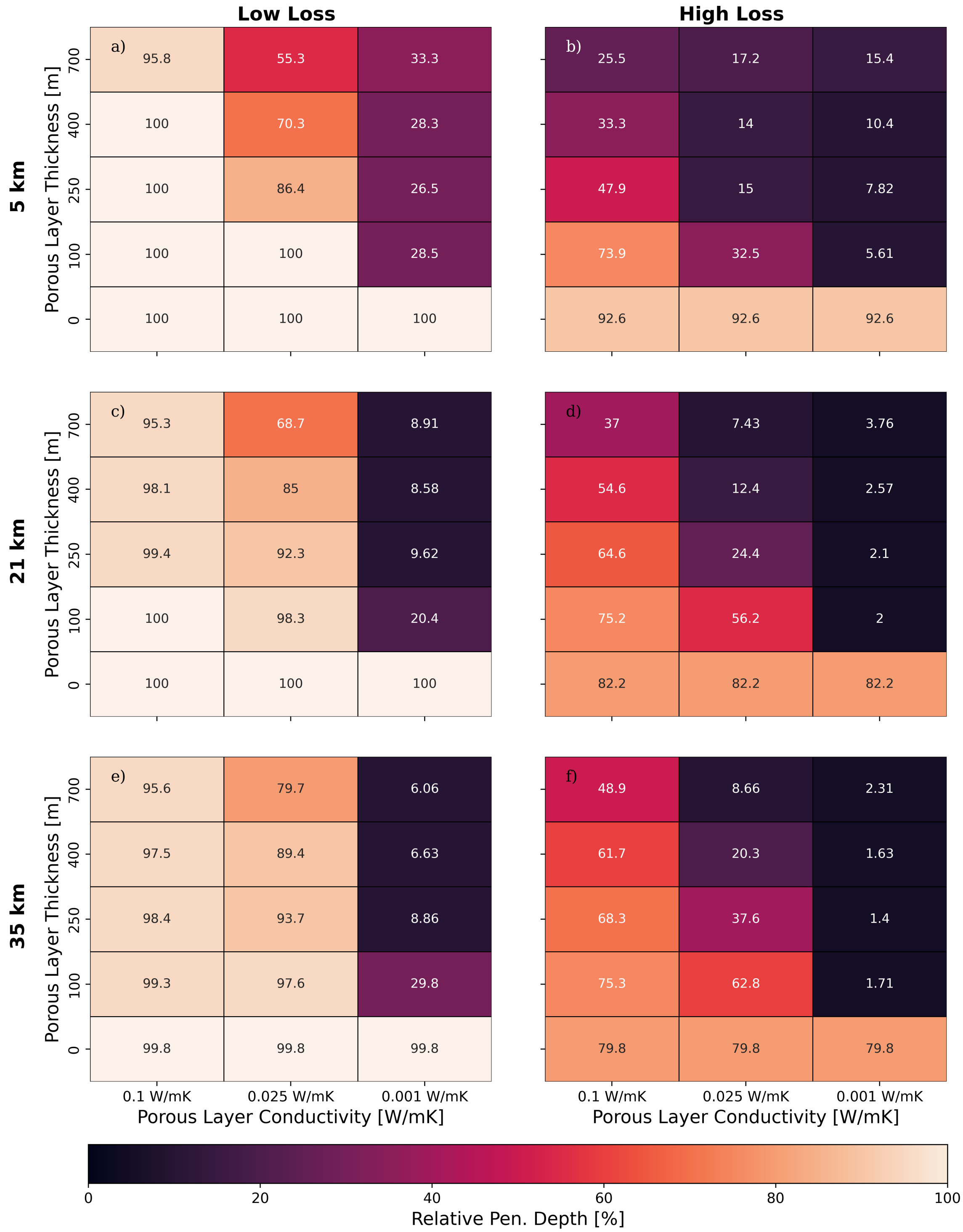

Figure 2.1: Similar as Fig. 2 in the main manuscript, but using a surface temperature of 85 K.

S3 Map of relative penetration depth

Here we repeat the analysis of the relative penetration depth presented in the main manuscript with and without the presence of a porous ice layer of various thickness for a more homogeneous ice shell thickness (Fig. 3.1). To this end, we chose the ice shell thickness model of *Hemingway and Mittal* (2019) that uses the shape model of *Tajeddine et al.* (2017), an ice density of 900 kg m^{-3}, and an ocean density of 1100 kg m^{-3}.

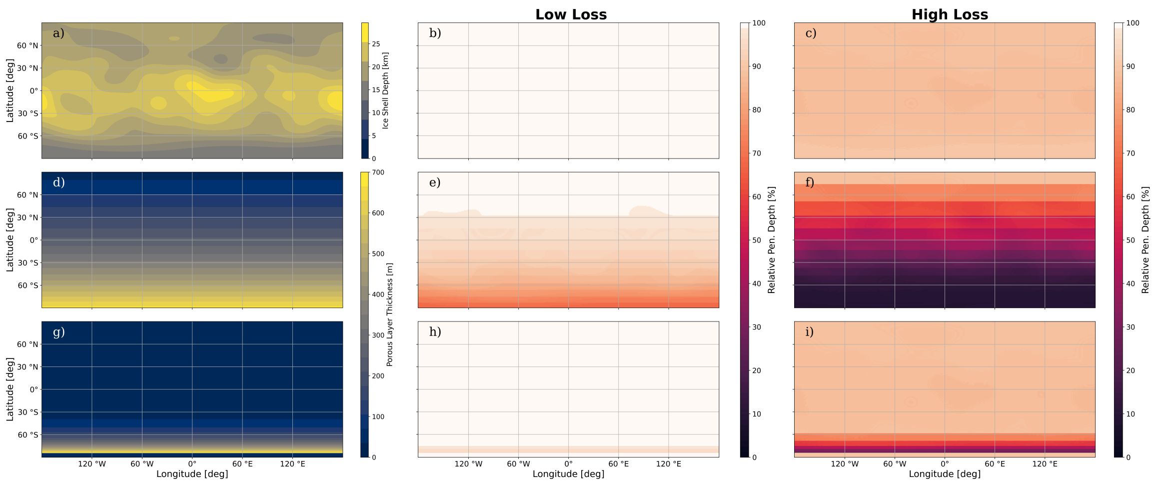

Figure 3.1: Maps of the: a) ice shell thickness *Hemingway and Mittal* (2019), b) porous layer distribution for b) the ”exponential-global distribution” (i.e., exponential decay from 700 m at the south pole to 20 m at the north pole), c) the ”exponential-hemispheric distribution” (i.e., exponential decay from 255 m at 85°S to 0 m at the equator). The radar penetration depth relative to the ice shell thickness in panel a) is shown for d) no porous layer, e) exponential-global and f) exponential-hemispheric distribution of the porous layer. Panels g), h) and i) are similar to d), e), and f), but show the high-loss cases.

Given the thicker ice shell at the south pole in this scenario compared to the map shown in Fig. 3 of the main manuscript, in none of the high-loss scenarios, with or without the presence of a porous ice layer, 100% relative penetration depth is reached. In the low-loss scenarios, the relative penetration depth reaches 100% almost everywhere for the ”no regolith” and the ”exponential-hemispheric distribution” cases. For the ”exponential-global distribution” scenario the relative penetration depth reaches 100% only for latitudes higher than 30°N.

S4 Depth to eutectic interfaces

In the following plots, we show maps containing the depth to the ammonia and ammonium chloride eutectic interfaces similar as in Fig. 4 of the main manuscript, but now using different ice shell thicknesses and distributions of the porous ice layer. The results show that in the low-loss scenario, the eutectic interfaces can be reached before the two-way attenuation increases to 100 dB, independently of the ice shell thickness or porous layer distribution. In the high-loss scenario, the eutectic interface of ammonium chloride is difficult to detect, unless the ice shell is thin (i.e., around 5 km, cf. Fig. 4.2).

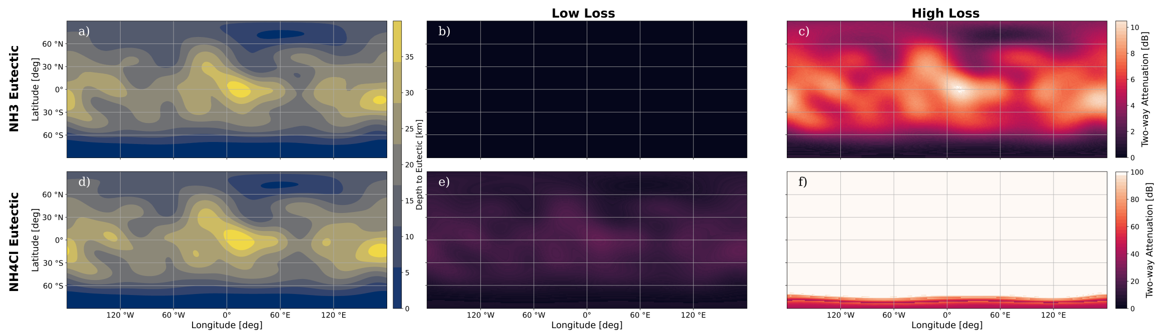

Figure 4.1: Maps showing the depth of: a) ammonia (NH_3) and b) ammonium chloride (NH_4Cl) eutectic interface for the same ice shell thickness used in Fig. 4 of the main manuscript but now without a porous ice layer. Panels c) and d) indicate the corresponding two-way attenuation values for the low-loss case at the eutectic interface of NH_3 and NH_4Cl, respectively. Panels e) and f) are similar to c) and d), but for the high-loss scenarios.

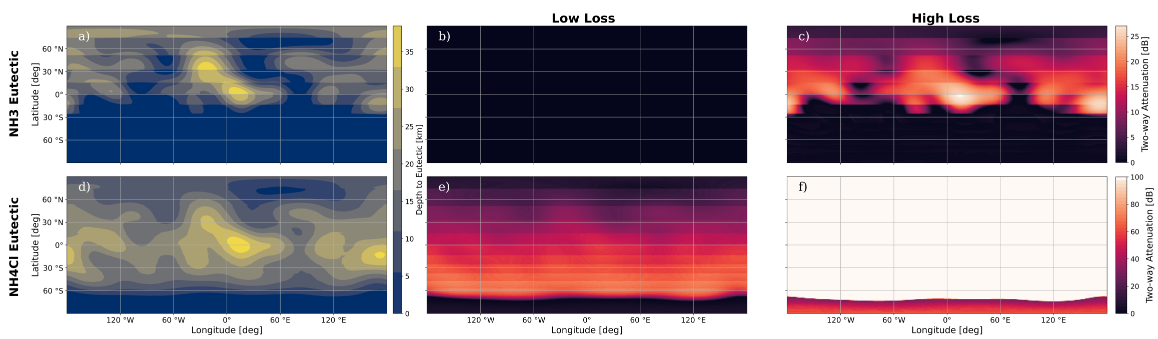

Figure 4.2: Same as Fig. 4.1 but using the "exponential-global distribution" of the porous ice layer. Panels c) and d) indicate the corresponding two-way attenuation values for the low-loss case at the eutectic interface of NH_3 and NH_4Cl, respectively. Panels e) and f) are similar to c) and d), but for the high-loss scenarios.

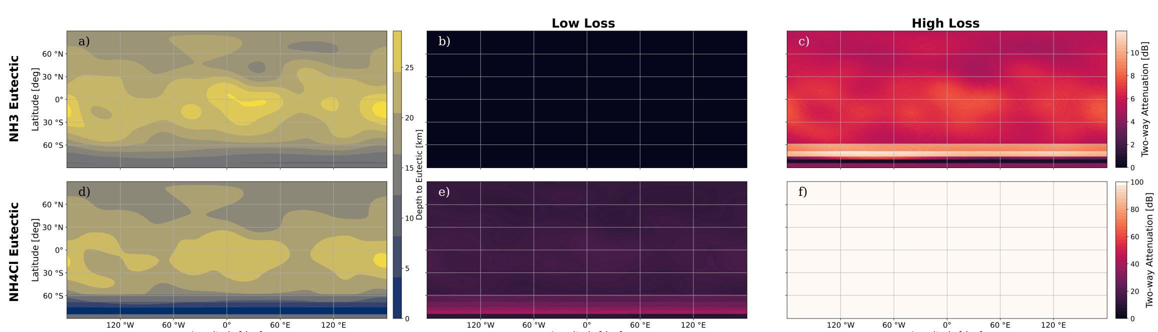

Figure 4.3: Same as Fig. 4.2 for the "exponential-hemispheric distribution" of the porous ice layer and a more homogeneous ice shell thickness that uses the shape model of *Tajeddine et al.* (2017) and assumes a density difference between the ice and ocean of 200 kg m^{-3} (*Hemingway and Mittal*, 2019).

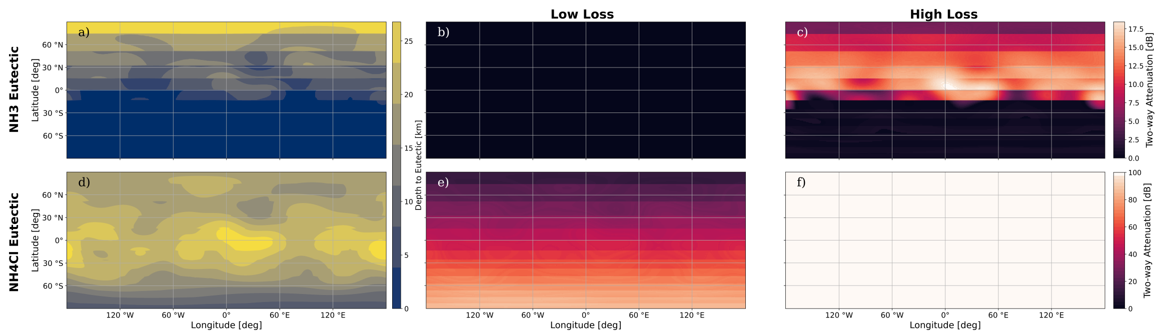

Figure 4.4: Same as Fig. 4.4 using an "exponential-global distribution" of the porous ice layer.

S5 Datasets

Additional datasets and the python scripts to reproduce the results presented in the main manuscript and supplementary material are available on Zenodo *Byrne et al.* (2024).

References

Byrne, W., A.-C. Plesa, T. Rückriemen-Bez, H. Hussmann, and A. Benedikter, Radar Attenuation for Subsurface Sounding on Enceladus: Effects of a Porous Ice Layer, doi: 10.5281/zenodo.10932227, 2024.

Hemingway, D. J., and T. Mittal, Enceladus's ice shell structure as a window on internal heat production, *Icarus*, *332*, 111–131, 2019.

Kalousová, K., D. M. Schroeder, and K. M. Soderlund, Radar attenuation in Europa's ice shell: Obstacles and opportunities for constraining the shell thickness and its thermal structure, *Journal of Geophysical Research: Planets*, *122*(3), 524–545, 2017.

Souček, O., M. Běhounková, D. M. Schroeder, N. S. Wolfenbarger, K. Kalousová, G. Steinbrügge, and K. M. Soderlund, Radar Attenuation in Enceladus' Ice Shell: Obstacles and Opportunities for Constraining Shell Thickness, Chemistry, and Thermal Structure, *Journal of Geophysical Research: Planets*, *128*(2), e2022JE007,626, 2023.

Spencer, J., J. Pearl, M. Segura, F. Flasar, A. Mamoutkine, P. Romani, B. Buratti, A. Hendrix, L. Spilker, and R. Lopes, Cassini encounters Enceladus: Background and the discovery of a south polar hot spot, *science*, *311*(5766), 1401–1405, 2006.

Tajeddine, R., K. M. Soderlund, P. C. Thomas, P. Helfenstein, M. M. Hedman, J. A. Burns, and P. M. Schenk, True polar wander of Enceladus from topographic data, *Icarus*, *295*, 46–60, 2017.